Review Article

Shailendra Chiluwal, Apparao M. Rao, and Ramakrishna Podila*

Strategies for improving rechargeable lithium-ion batteries: From active materials to CO_2 emissions

https://doi.org/10.1515/ntrev-2021-0114
received March 17, 2021; accepted October 17, 2021

Abstract: The recent past witnessed rapid strides in the development of lithium-based rechargeable batteries. Here, some key technological developments in intercalation, conversion, and alloy-type anode and cathode materials are reviewed. Beyond the active electrode materials, we also discuss strategies for improving electrolytes and current collectors. An outlook with remarks on easily misleading battery characteristics reported in the literature, impending challenges, and future directions in lithium-based rechargeable batteries is provided. Lastly, the authors also emphasize the need for lab-based research at the pouch cell level with practical energy densities, in addition to discussing scalability and economic viability of different battery materials and their architectures.

Keywords: rechargeable lithium-ion batteries, active materials, CO_2 emission

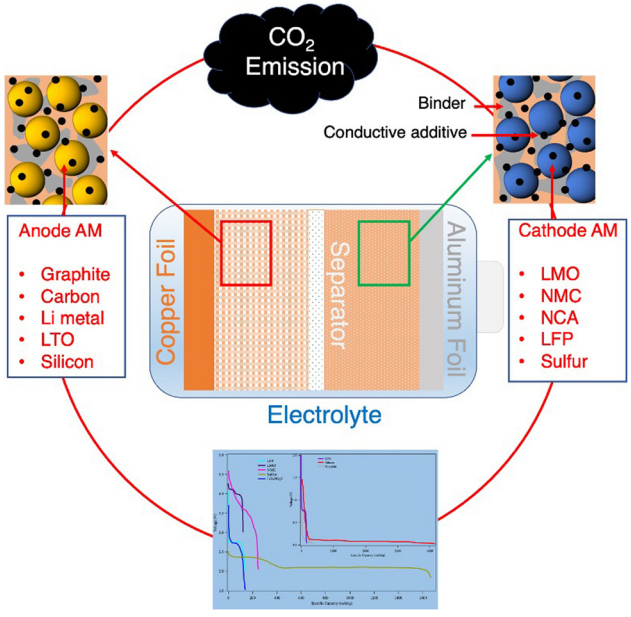

Graphical abstract

1 Introduction

Alternative vehicle technologies, such as battery electric vehicles (BEVs), are being developed to reduce our dependence on oil for transportation and mitigate CO_2 emissions [1–4]. Unlike low-efficiency gasoline or diesel-based internal combustion engines that power most present-day vehicles, a BEV is fully powered by the energy stored in a large onboard battery pack with projected efficiencies up to 70%. The performance of a BEV ultimately hinges on the power and energy capacity of its battery pack. An automotive battery pack typically consists of a large number of cells (few hundreds to thousands) to meet the required energy and power needs of a BEV. The wide deployment of BEVs for maximizing the electrification of the road transportation system demands drastic improvements in the performance of today's battery packs. Specifically, the U.S. Advanced Battery Consortium developed a set of goals for BEV battery packs, which require that the specific energy be increased beyond 235 W h/kg at the pack level (with a concomitant volumetric energy density of 500 W h/L) at power densities as high as 2,000 W/kg while reducing the cost to <$125 per kW h [5].

The automotive and electronic industries have embraced rechargeable lithium-ion battery (LIB; Figure 1a) as "the component" for battery packs because it provides the highest energy density of all commercially available battery chemistries [1,6,7]. Although presently used 85 kW h LIB-based

* **Corresponding author: Ramakrishna Podila,** Department of Physics and Astronomy, Clemson Nanomaterials Institute, Clemson University, Clemson, SC, 29634, United States of America, e-mail: rpodila@g.clemson.edu
Shailendra Chiluwal, Apparao M. Rao: Department of Physics and Astronomy, Clemson Nanomaterials Institute, Clemson University, Clemson, SC, 29634, United States of America

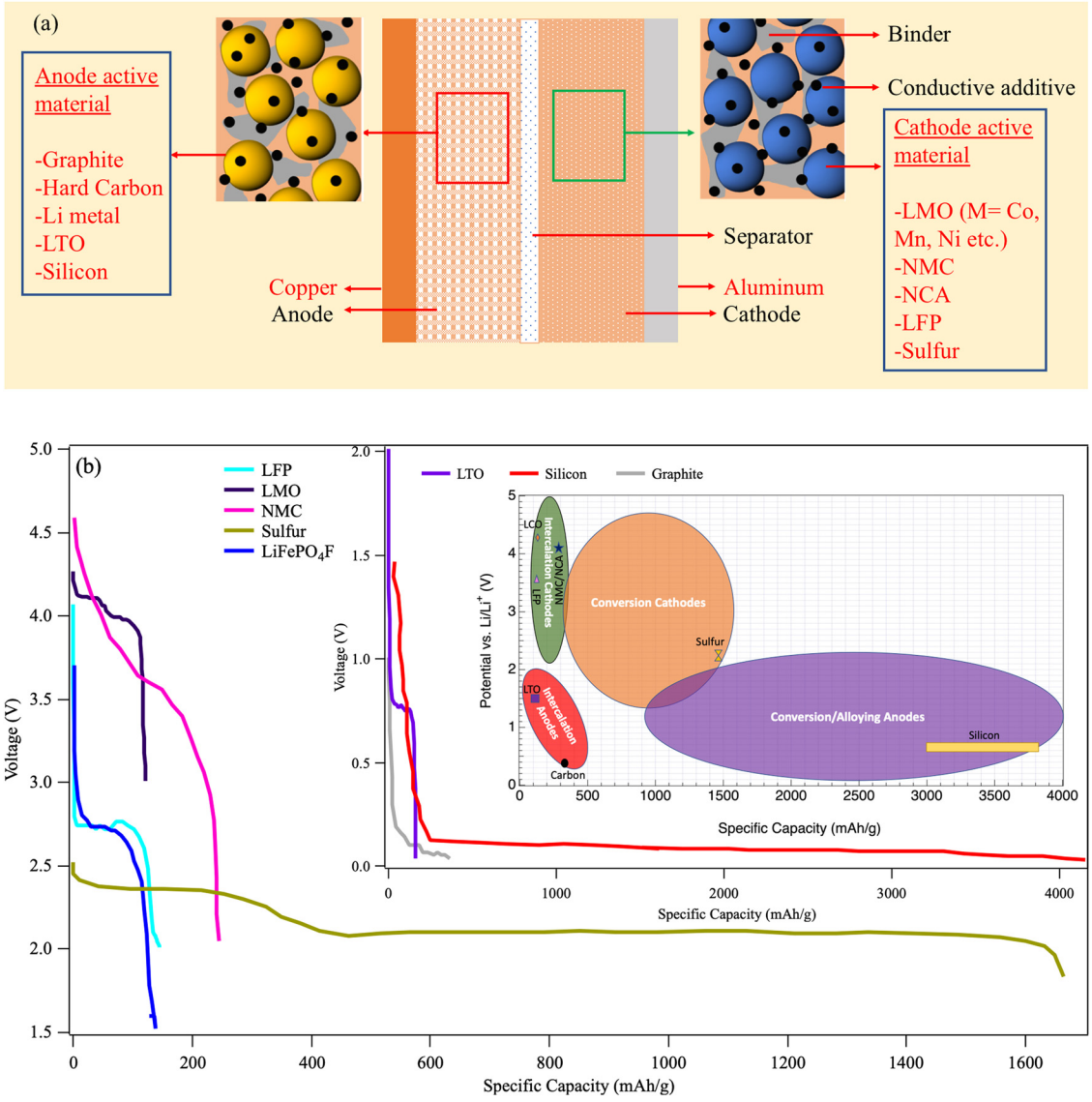

Figure 1: (a) A schematic showing the components of Li-ion batteries. Novel strategies to improve LIB performance by optimizing different components of LIB (red text) will be discussed in this review. (b) Approximate behavior of theoretical discharge curves for selected cathode (inset-anode) materials. The inner inset shows the approximate ranges for average discharge potentials and specific/gravimetric capacities for intercalation and conversion/alloy type electrodes. Some widely used or promising electrode materials that are highlighted in this review are also shown ($Li_4Ti_5O_{12}$ (LTO): $Li_4Ti_5O_{12}$; $LiFePO_4$ (LFP): $LiFePO_4$; $LiCoO_2$ (LCO): $LiCoO_2$; nickel manganese cobalt oxide (NMC): $LiNi_{0.33}Co_{0.33}Mn_{0.33}O_2$; NCA: $LiNi_{0.8}Co_{0.15}Al_{0.05}O_2$).

packs allow up to ~250 miles driving range on a single charge, their cost is twice the price of a standard economy car. The high cost and limited mileage of present LIB-powered cars are due to the intrinsically limited capacities of the Li-ion insertion cathodes, which are nearing their practical limits. While much progress is being made to improve LIBs, other battery chemistries such as lithium–sulfur batteries (LSBs), Al-ion, Na-ion, and K-ion are also being explored [8–14]. In this short review, recent progress in improving the electrochemical performance and cycle life of lithium batteries is presented.

Given that lithium batteries can deliver higher energy and power densities, they were the obvious choice for portable electrochemical energy storage. In the recent past, much research has been devoted to realizing LIB electrodes with higher rate capability and charge capacity. For LIB cathodes, achieving sufficiently high voltage can drastically improve their energy and power densities and make them smaller and cheaper. Figure 1b shows the general range of different intercalation and conversion/alloying-type cathodes and anodes for LIBs. This review discusses efforts to improve lithium battery electrodes at

various levels *via*: (1) the identification of the optimal chemical composition of active materials (AMs), (2) tailoring physical properties of AMs such as size and surface, and (3) integrating AMs with binders, conductive additives, and current collectors. More importantly, this review will also discuss how different interfaces such as the solid electrolyte interface (SEI) and current collector active material interface (CCAMI) impact the LIB performance and highlight strategies to overcome adverse interfacial effects.

2 Intercalation cathodes

The LIB intercalation cathodes can be categorized into four different crystal structures, *viz*., layered, spinel, olivine, and tavorite [15,16]. Although many materials can be used as intercalation cathodes, much attention has been paid to transition metal oxide and polyanion compounds because of their higher operating voltages [17]. These oxide cathodes can deliver specific capacities ~150–200 mA h/g at the cathode level. To increase the specific capacity and cycling stability, much research has been devoted to identifying the optimal chemical composition for achieving high specific capacity in intercalating AMs.

2.1 Layered intercalation cathodes

The first intercalation cathode ($LiTiS_2$) was developed by Whittingham and Gamble in 1975 [18], but due to a lower voltage (~2 V), these cathodes were replaced by layered intercalation metal oxide cathodes ($LiMO_2$, M is either bulk transition metal or a mixture of different transition metals) [18]. These cathodes have high operating voltage (3.0–4.8 V) and high theoretical specific capacity (~250–280 mA h/g). Goodenough, the 2019 Nobel Laureate in Chemistry, introduced LCO as an alternative cathode that was eventually commercialized by SONY [19]. Although it exhibited high capacity (~275 mA h/g), the cost of Co is high. Also, at higher voltages, LCO suffers from a fast capacity fade due to the structural changes within the material [20–22]. Additionally, its thermal instability limits its use in EVs [17,23]. The use of other isostructural oxides has also been explored, for example, $LiNiO_2$ (LNO) is a cheaper alternative to LCO with a comparable theoretical specific capacity. However, LNO is difficult to synthesize [24,25] and is thermally unstable [26]. Another cheaper and environmentally friendly alternative to both LCO and LNO is $LiMnO_2$ (specific capacity ~285 mA h/g), which too is difficult to synthesize and suffers from high capacity fading due to a change in its crystal structure from layered to spinel ($LiMn_2O_4$) with cycling [17,27–33]. Subsequent studies found that the presence of dopants in $LiMnO_2$ helped reduce the thermal runaway and enhance structural stability and cycling stability at higher voltages [34–38]. Consequently, ternary materials such as $LiNi_xCo_yMn_zO_2$ (often referred to as NCM or NMC) and $LiNi_{0.8}Co_{0.15}Al_{0.05}O_2$ (NCA) were developed, which proved attractive for commercial use. For example, NMC proved as a cheaper alternative compared to LCO as it contained a minimal amount of Co and exhibited a relatively superior thermal stability and a similar or higher specific capacity compared to LCO at the same operating voltage [39]. $LiNi_{0.33}Co_{0.33}Mn_{0.33}O_2$ (also known as NMC 111) is the common form of NMC that is widely used in today's battery market. Beyond the NMC 111 composition, higher specific capacities were achieved in Ni-rich NMC cathode materials; however, they suffered from poor thermal stability and cycle life [40,41]. Similar to NMC, NCA is another cathode AM in which Ni is substituted with small amounts of Co and Al, and Al is known to improve the thermal stability of NCA [42]. The theoretical capacity of NCA is ~280 mA h/g [42], and both Panasonic and Tesla have embraced NCA over LCO as the cathode material for their LIBs. Lastly, a small amount of ion doping (Cl, Mg, Na, F, *etc*.) has also been shown to improve the thermal stability of NCA [24,36–60].

Recently, another family of Li-rich layered oxide composite has been synthesized by structurally incorporating a Li_2MnO_3 stabilizer into an electrochemically active $LiXO_2$ host (X = Mn, Ni, Co). The excess lithium in such Li-rich oxide composites boosts the specific capacity of the cell up to ~460 mA h/g (for Li_2MnO_3) by activating Li_2MnO_3 at >4.5 V [68]. Such activation releases Li_2O initially and facilitates better Li diffusion by acting as a Li reservoir. $LiXO_2$ are cost effective and environmentally friendly [69], and although they exhibit a relatively higher capacity they are considered to be electrochemically inactive (Table 1). Accordingly, much effort has been devoted to increase their electrochemical performance through ion doping (Ni, Mg, Ru, Cr, Mo *etc*.) [63–75,17].

2.2 Spinel intercalation cathodes

In 1983, Thackeray *et al*. proposed that $LiMn_2O_4$ (LMO) [88] (specific capacity ~150 mA h/g) could be used as an intercalating cathode. LMO exhibits a cubic "spinel"

Table 1: Representative layered intercalation cathode materials along with their operating voltage, cycle capacity, and C rate

Material	Operating voltage (V)	Initial/final capacity (mA h/g)	Cycle/C rate	Year/Ref.
LCO	2.7–4.3	145/140	20/1C	2003 [83]
NMC 111	3.0–4.3	150/150	10/0.5C	2013 [84]
NCA	3.0–4.3	184.5/172.3	110/1C	2018 [85]
NMC 622	3.0–4.2	155.4/147.3	400/0.1C	2017 [86]
NMC 811	3.0–4.2	172.5/114.7	400/0.1C	2017 [86]
$LiNi_{0.8(1-x)}Co_{0.1}Mn_{0.1}Ca_{0.8x}O_2$	2.5–4.5	195/130	100/0.2C	2017 [64]
$Li(Ni_{0.5}Co_{0.2}Mn_{0.3})_{1-x}Zr_xO_2$	3.0–4.6	190/166	100/1C	2016 [54]
Li_2MnO_3	2.0–4.8	180/NA	NA	2013 [87]
$Li_{1.98}Mg_{0.01}MnO_3$	2.0–4.6	307.5/259.8	30/0.1C	2016 [79]
$Li_{1.23}Fe_{0.15}Ni_{0.15}Mn_{0.46}O_2$	1.5–4.5	255/211	50/NA	2017 [78]

structure in which Li is present at tetrahedral sites and Mn at the octahedral sites. LMO is relatively cheaper and environmentally friendly; however, its cycling stability is poor because Mn tends to dissolve in electrolytes such as $LiPF_6$ [89,90] and $LiAsF_6$ [89,90]. Surface coating [91–96], tuning morphology and size [97–99], and doping [100–104] have been found to increase the cycling stability of LMO. Particularly, Ni-substituted ($LiMn_{2-x}Ni_xO_4$) and ($Li_x(MnNi)_{1-x}O_4$) spinels have emerged as promising cathode materials (Table 2) as they exhibit excellent cycling stability even at a high potential (~4.8–5.0 V) [105–107].

2.3 Olivine intercalation cathodes

Olivine phosphates ($LiMPO_4$) [109] and olivine silicates (Li_2MSiO_4) [110], where M = Fe, Mn, Mg, and Co, have also been evaluated as cathode materials [42,111]. Unlike the layered LCO and LNO cathodes, olivine electrodes are significantly more stable and exhibit better power capability [17]. Although LFP has been used in commercial LIBs, it exhibits a relatively low open circuit potential (3.5 V) and low electrical/ionic conductivity [111]. As such, surface coatings and dopants have been used to increase the conductivity of the LFP [112–115]. Notably, as discussed later in Section 2.6, a new approach involving Al current collector with vertically aligned carbon nanotubes (VACNTs) could resolve the CCAMI issue and improve conductivity across the interface between LFP and the Al current collector [116]. Other olivine-like materials such as $LiNiPO_4$, $LiMnPO_4$, $LiMgPO_4$, and $LiCoPO_4$ also have a higher potential (4.1–4.8 V) but they exhibit a high intrinsic resistance which results in lower electrochemical activity and capacity [117–119]. Similar CCAMI approaches as in the case of LFP were used to improve the electrochemical activity and capacity [117,120,121]. Olivine silicates are more thermally stable than phosphates as all four oxygen atoms of tetrahedron SiO_4 contribute to connect the structural framework, whereas in phosphate only three oxygen atoms contribute [122]. Also, the theoretical capacity of silicates is almost double (~330 mA h/g) that of LFP [123–125]; however, the practical cycling performance of these silicates is not comparable to that of LFP because of its structural instability/phase change during charging [126–128]. Excess lithium was found to improve structural stability [129], specifically Li_xMSiO_4 (where $x = 2$), which was modified using approaches similar to those used for LFP to increase the overall electrochemical performance (Table 3) [122,130–132].

Table 2: Representative spinel intercalation cathode materials along with their operating voltage, cycle capacity, and C rate

Material/condition	Operating voltage (V)	Initial/final capacity (mA h/g)	Cycle/C rate	Year/Ref.
$LiMn_2O_4$/pure	3.0–4.5	96.00/85.15	100/1C	2019 [97]
$LiMn_2O_4$/LaF_3 coated	0–1.1	109.5/107.9	100/10C	2016 [108]
$LiMn_2O_4$ nanorods/$Li_4Ti_5O_{12}$ coated	3.2–4.2	98.4/80.9	500/1C	2019 [98]
$LiMn_2O_4$/mesoporous	3.0–4.5	100.51/96.42	100/1C	2019 [97]
$LiMn_2O_4$/Al doped	3.2–4.2	100.7/94.6	400/0.5C	2020 [104]
$LiMn_{1.5}Ni_{0.5}O_4$	3.5–5.0	111.4/102.3	50/5C	2010 [106]
$Li_{1.2}Mn_{0.6}Ni_{0.2}O_2$	2.0–4.8	>200/200	50/NA	2016 [107]

Table 3: Representative olivine intercalation cathode materials along with their operating voltage, cycle capacity, and C rate

Material/condition	Operating voltage (V)	Initial/final capacity (mA h/g)	Cycle/C rate	Year/Ref.
$LiFePO_4$	2.0–4.0	117/113	50/0.1C	2019 [115]
$LiFePO_4$/$GdPO_4$ and C coating	2.0–4.0	158/157	50/0.1C	2019 [115]
$LiFePO_4$/Ti doped	2.3–4.2	155/150	500/1C	2020 [112]
$LiMnPO_4$/C	2.5–4.5	105/100	50/0.05C	2017 [120]
$LiMn_{0.99}Y_{0.01}PO_4$/C	2.5–4.5	153.6/148.1	50/0.05C	2017 [120]
Li_2FeSiO_4/C	1.5/4.5	134/155	190/0.2C	2010 [129]
Li_2MnSiO_4/C	1.5–4.8	280/120	16/NA	2020 [130]

2.4 Tavorite intercalation cathodes

Considering their exceptional thermal stability and ionic conductivity, tavorite intercalation cathodes ($LiMPO_4F$) are a suitable replacement for olivine cathodes. Tavorite cathodes allow 3D ion transport unlike 1D transport in olivine cathodes [12,133]. Materials with an open structure, such as $LiFeSO_4F$/$LiVPO_4F$/$LiVPO_4O$ (specific capacity ~150 mA h/g) have been considered as promising cathodes as they exhibit an open circuit potential (>4 V) in addition to a stable structure that supports fast Li-ion diffusion (Table 4) [52,133–137]. Although the stability is better, the synthesis of these materials in their pure form remains challenging [135,138].

2.5 Nanostructured intercalating AMs for cathodes

The recent progress in lithium batteries has largely benefited from the development of nanostructured electrodes in comparison to conventional electrodes because of their unique morphology, significantly enhanced kinetics, and large surface area (Table 5) [3,6,17,140–151]. Nanostructured electrodes shorten the diffusion length and facilitate a higher contact area between the electrolyte and AMs leading to more exposed redox sites, which deliver higher power and energy densities [144,152–154]. Fick's correlation between the diffusion length L and its diffusion coefficient D can be expressed as $\tau = L^2/D$ [144], where τ is the diffusion time.

Based on the Li-ion diffusion coefficient $D = 2.5 \times 10^{-12}$ cm^2/s, a complete discharge occurs within ~40 s when the particle size is $L = 100$ nm while it takes ~1 h for $L = 2$ µm. Many physicochemical characteristics such as crystallinity, phase purity, particle morphology, grain size, and surface area depend largely on the AM synthesis methods. Thus, different fabrication methods such as grinding, ball milling, and sol–gel method have been used to synthesize nanostructured intercalating AMs. A detailed review on the synthesis methods can be found in ref. [155].

Okubo *et al.* [156] demonstrated excellent high-rate capability for nanosized LCO (average particle size ~17 nm), that is, 65% of the 1C-rate capability retention. However, they also found that extreme reductions in the crystallite size below 15 nm drastically decreased the overall capacity plausibly due to defects. In the case of LFP, the capacity increased linearly with decreasing particle size [152]. In the case of LMO, though the initial capacity was higher, increased capacity fading was observed due to the dissolution of Mn into electrolyte *via* disproportionation reaction on the larger surface area nanostructured LMO [157–160]. Although nanostructuring can reduce Li^+ diffusion length ensuring an improved rate capability, it increases the oxidation of nanoparticles (NPs) leading to a thicker SEI layer on the surface of the electrode and results in capacity fading [153,154]. As discussed in the previous section, both size and structure of AM play a critical role in improving the

Table 4: Representative tavorite intercalation cathode materials along with their operating voltage, cycle capacity, and C rate

Material/condition	Operating voltage (V)	Initial/final capacity (mA h/g)	Cycle/C rate	Year/Ref.
$LiFePO_4F$	1.5–4.0	110.2/91.5	300/0.5C	2018 [138]
$LiFePO_4F$/Ag decorated	1.5–4.0	120.3/115.5	300/0.5C	2018 [138]
$LiFePO_4F$ nanospheres	1.5–4.0	110/104	200/0.5C	2018 [12]
$LiVPO_4F$/C	2.5–4.6	126.6/116.7	125/1C	2018 [139]
$Li_{0.99}K_{0.01}VPO_4F$/C	2.5–4.6	131.9/126.8	125/1C	2018 [139]

Table 5: Representative performance of nanostructured AMs

Material	Operating voltage (V)	Initial/final capacity (mA h/g)	Cycle/C rate	Particle size or morphology	Year/Ref.
$LiFePO_4$	2.5–4.0	163/163	1/1C	30 nm	2006 [194]
$LiFePO_4$	2.8–4.2	130/130	1/1C	150 nm	2006 [195]
$LiFePO_4$	2.0–4.5	115/115	1/1C	500 nm	2003 [196]
$LiFePO_4$	2.1–4.5	82/82	1/1C	800 nm	2006 [197]
$Li_{1.2}Mn_{0.54}Ni_{0.13}Co_{0.13}O_2$	2.0–4.8	153.9/136.7	300/3C	Nanotubes	2016 [177]
$LiMnPO_4/C$	2.5–4.5	123/120	100/1C	Nanorods	2018 [163]
$Li_{1.2}Mn_{0.54}Ni_{0.13}Co_{0.13}O_2$	2.0–4.8	138/121	100/10C	Nanowires	2019 [171]
$LiCoPO_4$	2.5–4.8	180/147	300/0.1C	Nanoplates	2016 [179]
$LiNi_{0.5}Mn_{1.5}O_4$	3.5–4.8	136/126	100/1C	Nanosheets	2019 [183]
$Li_{1.2}Mn_{0.6}Ni_{0.2}O_2$	2.0–4.8	197.3/174.6	200/1C	3D micro/nano	2019 [185]
$Li_{1.16}Mn_{0.6}Ni_{0.12}Co_{0.12}O_2$	2.0–4.8	227/213	50/5C	3D micro/nano	2017 [187]

electrode performance. Recent efforts have focused on 1D morphologies such as nanorods [161–167], nanowires [168–174], and nanotubes [175–178] as they can effectively accommodate volume changes during lithiation/delithiation in addition to promoting diffusion and structural stability [152,174].

Two-dimensional cathode materials with high specific areas are of interest because they provide open 2D channels for Li-ion transport and show better stability than that of the 0D and 1D particles. Although most of the research on 2D electrodes has focused on anode materials, a few reports focused on $LMPO_4$ [117,179–183] 2D cathodes, mostly plausibly due to the unavailability of simple and cost-effective ways of synthesizing 2D cathode materials [181]. Zhao *et al.* [183] prepared flower-like $LiNi_{0.5}Mn_{1.5}O_4$ nanosheets, which delivered a capacity of 142 mA h/g at 1-C-rate after 100 cycles at 55°C. The LMO microsheets synthesized using a simple carbon gel-combustion synthesis method delivered 91 mA h/g after 300 cycles at 10C [184]. Many challenges such as high preparation cost, low packing density, and inevitable particle aggregation have hampered the use of nanomaterials. Novel 3D hierarchical micro/nanoarchitectures have also been used to improve cell performance [184–193]. Such structures are micron-scale assemblies comprising nanoscale building blocks that enable better electrochemical performance and structural stability [185]. A detailed review of such architectures could be found elsewhere [152].

2.6 Integrating AMs with conductive additives

Most AMs used in LIB electrodes (both anodes and cathodes) are poor electrical conductors and are often mixed with conductive additives (*e.g.*, conductive carbon black often referred to as Super P) [142,198]. In a typical LIB cathode (/anode) manufacturing line, the Al (/Cu) current collector is coated with a slurry containing AM and conductive additives and a binder such as polyvinylidene fluoride or PVDF in *N*-methyl-2-pyrrolidone (NMP) [199]. Although carbon black (*e.g.*, Super P) is widely used as a conductive additive, other carbon nanomaterials such as graphene, CNTs, and reduced graphene oxide (rGO) have shown great promise in improving the specific capacity (Table 6) [200–216]. When carbon-based additives are

Table 6: Representative electrochemical performance of intercalating AM cathodes made by integrating conductive additives

Material	Conductive carbon additive	Operating voltage (V)	Initial/final capacity (mA h/g)	Cycle/C rate	Year/Ref.
$LiFePO_4$	Carbon	2.5–4.2	144/138	100/0.5C	2017 [207]
$LiFePO_4$	N-carbon and rGO	2.0–4.2	116/112	700/10C	2017 [219]
$LiFePO_4$	3D graphene	2.4–4.2	141.1/139.8	600/10C	2018 [220]
NCA	Carbon nanotubes	2.8–4.5	187/181	60/0.25C	2017 [200]
Li_2MnO_3	rGO	2.0–4.6	290/250	45/0.1C	2017 [221]
$LiMn_2O_4$	Carbon and carbon nanofibers	3.0–4.3	120/92	1,000/1C	2020 [222]
NMC	Graphene	2.7–4.2	140/103	500/1C	2017 [223]
$LiMn_{0.8}Fe_{0.2}PO_4$	Carbon/N-rGO	2.0–4.6	156.9/145.5	100/0.2C	2019 [224]

used, one should be aware of the fact that such additives could reduce the tap density and affect Li-ion transport. Thus, the use of the minimum amount of additives is suggested [217,218].

2.7 Modifying/replacing traditional Al current collectors for cathodes

Although Al foils are widely used as the cathode current collector, there are several drawbacks such as localized corrosion due to electrolyte, weak adhesion to AMs, and limited contact area [225,226], which adversely affect the electrochemical performance of cells. To improve AM adhesion to Al-foils, the surface is often treated chemically or modified [227–231]. As shown in Figure 2, the total internal resistance of LIBs arises due to the existence of the interfaces between AM, binder, conductive additives, and the current collector. An increase in the internal resistance could decrease the overall electrochemical activity [232]. As described in Sections 2.1–2.5, the present LIB literature is replete with different procedures for improving the interfaces within the active materials using nano/micro-structuring or adding novel conductive additives such as carbon black, graphene, and rGO [2,233]. While conductive carbon additives decrease the resistance of interfaces within the cathode/anode active material, they are ineffective in decreasing the current collector active material interface or CCAMI resistance (see Figure 2) – *a key driving factor for increasing energy and power densities* that has largely been ignored in LIBs [234].

Ventrapragada *et al.* [116] extensively investigated the role of CCAMI resistance by using VACNTs, either directly grown or spray coated on Al foils. The CCAMI resistance of traditional LFP and NMC electrodes coated on Al/VACNT current collector was reduced by a factor of 3 in comparison to bare Al foil. Moreover, the capillary channels provided by the VACNTs grown on the Al foil promotes the wettability of aqueous slurry due to an increase in surface roughness, thus alleviating the need for toxic organic solvents (*e.g.*, NMP) to prepare the AM slurry. CNT-coated electrodes displayed energy densities as high as follows: ~500 W h/kg at 170 W/kg for LFP and ~760 W h/kg at ~570 W/kg for NMC. The CCAMI engineered LIBs exhibited an initial capacity of ~103 mA h/g with a capacity retention of ~80% at 4C after 500 cycles, unlike the commercial electrodes that could not withstand such a high C-rate. By using the carbon black and graphene-modified Al-foil (CG-Al) for the LFP electrode, Wang *et al.* [228] also demonstrated superior performance over the bare Al-foil (B–Al). The capacity retention at 1C-rate after 500 cycles of CG–Al–LFP battery was ~94% with initial capacity ~154 mA h/g, whereas, for B-Al-LFP, the capacity retention was ~90% with initial capacity ~120 mA h/g. Interestingly, Loghavi *et al.* treated the Al surface with a combination of three acids and observed an increase in capacity over the untreated Al foil [229].

There has been a growing interest in displacing relatively heavy metallic current collectors in LIBs with lightweight, low cost, and highly conductive materials that can satisfy the robustness as well as high utility requirement of LIBs (Table 7) [226]. Lightweight and flexible carbon-based current collectors have been researched because of their wide electrochemical window. Using graphene foil as a current collector for NMC523 cathode, Xu *et al.* [226] reported a ~45% increase in gravimetric capacity at the electrode level compared to bare Al foil

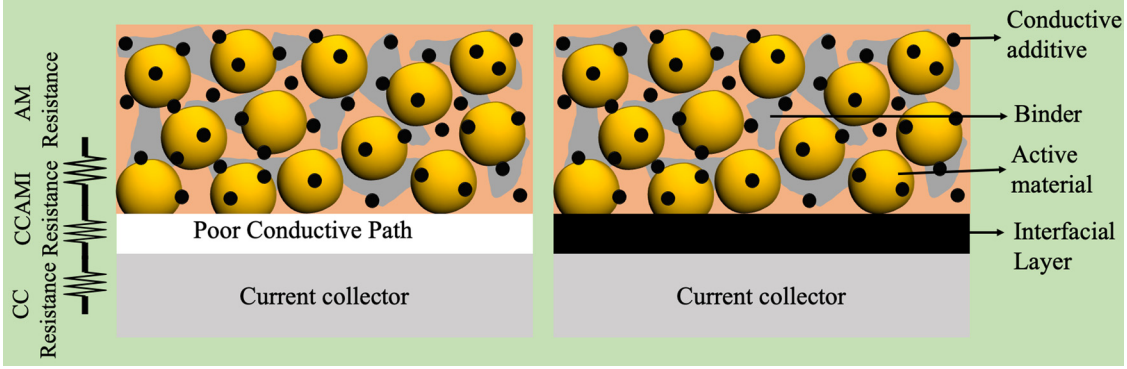

Figure 2: Various resistances in a cathode/anode electrode (left – traditional electrode, right – CCAMI engineered electrode). An interfacial layer of carbon, CNTs, and VACNTs enables better electrical contact between the AM and the current collector (CC), which improves the electrochemical performance of the electrode.

Table 7: Representative electrochemical performance of cathodes depending on current collector

Material	Current collector	Operating voltage (V)	Initial/final capacity (mA h/g)	Cycle/C rate	Year/Ref.
$LiMnO_4$	Bare Al	3.0–4.4	101/76	360/0.5C	2017 [231]
$LiMn_2O_4$	Graphene/Al	3.0–4.4	100/91	360/0.5C	2017 [231]
LFP	CNT/Al	2.0–4.2	103/79	500/4C	2018 [116]
NCA	Acid treated Al	2.8–4.2	187/170	80/0.5C	2019 [229]
NMC523	Graphene foil	2.8–4.5	112.4/42.0	200/5C	2020 [226]
$Li_{1.2}Mn_{0.6}Ni_{0.2}O_2$	Carbon cloth	2.0–4.8	78/78	100/5C	2017 [237]
LFP	CNT/printing paper	2.0–4.2	135/90	450/1C	2019 [246]

current collector at 0.5C after 200 cycles. The energy density of graphene foil was ~350 W h/kg after 200 cycles at 0.5C higher than the bare Al foil that showed ~240 W h/kg. The use of carbon paper [235], carbon fiber [236], and carbon cloth [237] in place of the Al foil have resulted in higher gravimetric and higher energy density. Another alternative for Al-based cathodes is paper/cellulose-based current collectors. Low cost of raw materials, ease of availability, and biodegradability of cellulose-based current collectors have attracted much attention. However, unlike Al foil, these current collectors are not highly conducting. In this regard, many researchers have endeavored to make cellulose fiber-based conducting composites or coat papers with different conducting materials (*e.g.*, activated carbon) using additives, which affects the gravimetric capacity as the amount of inactive material is increased [238–245]. Ventrapragada *et al.* [246] prepared additive-free paper-CNT current collectors by spray coating CNTs on cellulose paper. Cells assembled using this current collector with LFP coating showed a high energy density of 460 W h/kg at a power density of 250 W/kg. These batteries were able to withstand a high current rate (4C) and showed cycling stability up to 450 cycles at 1C-rate. Wang *et al.* [237] developed a carbon cloth-based $Li_{1.2}Mn_{0.6}Ni_{0.2}O_2$ electrode, which performed better than commercial Al-foil at a high C-rate (5C).

3 Conversion-type cathodes

Since SONY's launch of the first commercial LIBs in 1991, researchers have endeavored to improve the performance of LIBs [6,247–250]. As the gravimetric energy densities of the state-of-the-art LIBs based on intercalating AMs (such as LFP [251], NCA [252], and NMC [86]) reached their practical limits, alternative conversion-type AMs have attracted much attention. Among all the existing conversion-type AMs, sulfur is one of the most promising candidates for the next-generation portable electronic devices owing to its high theoretical gravimetric capacity (1,675 mA h/g) and gravimetric energy density of 2,500 W h/kg (practical energy densities of 400–600 W h/kg at the cell level for lithium-sulfur batteries, or LSBs) in addition to low cost and abundance of sulfur [253]. However, there are many challenges impeding the practical applications of LSBs such as the following: (1) insulating nature of sulfur (S_8) and its discharge product (Li_2S), (2) polysulfide intermediates resulting in a loss of active material, (3) dendrite formation and unstable SEI leading to the consumption of electrolyte and lithium, (4) low areal capacity of the LSBs due to low sulfur-loadings; and (5) usage of binder, carbon additives and heavy current collector leading to low gravimetric capacity. To overcome these challenges, many efforts have been made as evident from the number of published review articles. From Google scholar search of keyword "lithium-sulfur review" and adjusting the timeline to "since 2019," we were able to find at least 20 review articles on LSBs, which address challenges presented earlier individually or collectively [254–274].

Although sulfur has a high theoretical capacity, its low electric conductivity ~5×10^{-30} S/cm (at 25°C) leads to its low utilization as an AM. In the past two decades, carbon-based conductive frameworks have been used for increasing the electrical conductivity of elemental sulfur-based cathodes. These hosts include materials such as carbon black [275–277] carbon fibers [278,279], carbon/graphene sheets [280–282], carbon nanotubes [281,283,284], and hollow porous carbon materials [285–289] The highly soluble polysulfide intermediates (LiS_x, $4 \le x \le 8$) generated during the reversible redox reaction between sulfur and its discharge product Li_2S (the so-called shuttle effect) lead to the continuous loss of the cathode AMs and degradation of the Li metal anode (Figure 3). Consequently, such elemental sulfur-based cathodes exhibit poor cycling stability and low Coulombic efficiency. These challenges have been addressed in two ways: (i) designing better carbon frameworks and (ii) replacing elemental sulfur with a sulfur-based polymer. Indeed, different carbon framework designs aimed toward suppressing the diffusion of polysulfide intermediates have been developed. Such designs include 1D permeable hollow

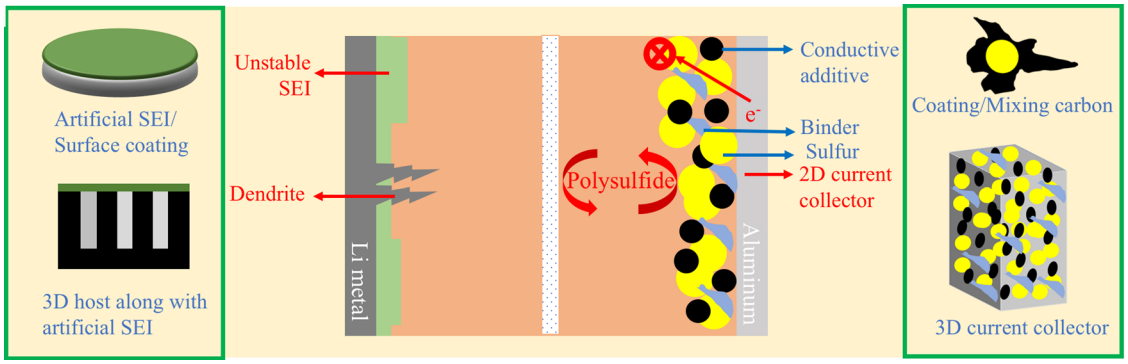

Figure 3: A schematic of a typical LSB battery is shown in middle. The red text corresponds to the challenges that are commonly reported in LSBs. The common solutions are shown in green boxes.

porous carbon shell cathode [290–296] and 2D conductive polymers or reduced graphene oxide nanosheets wrapped cathode [281,297–301]. Although physically confining sulfur could effectively reduce the outward diffusion of the polysulfides, the weak interaction between the nonpolar carbon and polar polysulfides prohibits the complete immobilization of polysulfides. Zhong *et al.* [275] prepared the popcorn-inspired macrocelluar carbon interconnected porous network that exhibited high electrical conductivity and was capable of blocking the polysulfide formation. N-doped carbon nanoflakes/carbon nanotubes can also decrease the polysulfide formation by decreasing the active sites for Li_2S decomposition [297,302,303]. Also, metal-organic frameworks in combination with carbon can increase the electrical conductivity and enable polysulfide immobilization [292,302,304–308].

Alternatively, polysulfide formation can be eliminated by using sulfurized polymers. Polyacrylonitrile (PAN) has been widely used as a carbon precursor for synthesizing porous carbon materials mainly due to its ease of dehydrogenation and cyclization into conjugated carbon backbones. The one-pot reaction of PAN with elemental sulfur provides a facile approach for the preparation of sulfurized PAN or SPAN. SPAN is a conductive sulfur-containing compound in which S atoms are covalently bonded to the polymer carbon matrix through a pyrolytic process. During sulfurization, sulfur acts as a mild oxidant to dehydrogenate PAN [309]. The structure and S content in SPAN depend on the pyrolysis temperature and duration. Based on extensive spectroscopic and theoretical studies, a few possible structures have been proposed as shown in Figure 4 [309]. Clearly, all possible SPAN structures do not exhibit the octagonal S_8 structure. Indeed, based on thermogravimetric analysis-mass spectrometry data, Zhang [309] proposed that Figure 4a is the most likely structure for SPAN obtained through pyrolysis at relatively lower temperatures (<600°C). In such structures, the lithiation of SPAN is expected to occur without the formation of any higher-order polysulfides, as shown in Figure 4d.

SPAN-based LSBs were first reported by Wang *et al.* [310], which was followed by He *et al.* [311,312] Beyond the one-pot reaction, Lai *et al.* [313] synthesized SPAN using a two-step technique by first pyrolyzing PAN and then reacting it with elemental sulfur. Their Li/SPAN cell with a 1 M $LiPF_6$ electrolyte showed a single discharge voltage plateau and a stable capacity of 770 mA h/g for 110 cycles at 40 mA/g. Similarly, Guo *et al.* [314] first pyrolyzed PAN into disordered amorphous carbon nanotubes and subsequently reacted them with sulfur at 500°C for 3 h. Their resulting SPAN tubes contained 40 wt% sulfur and were thermally stable up to 700°C suggesting that sulfur was covalently bonded to carbon as shown in Figure 4a–c. Moreover, their Li/SPAN cell showed stable capacities of nearly 700 mA h/g for 100 cycles at 10 mA/g. Ahn *et al.* and Ming *et al.* [315,316] also reported that the polysulfide intermediates could be eliminated by using SPAN as the cathode material. Although SPAN provides a stable conversion-type sulfur cathode, its use is limited by its poor ionic and electronic conductivities, which can be improved using carbon-based additives [317–322].

To increase the cycling stability with Li metal anode in LSBs, an electrolyte that is capable of forming a stable SEI layer is needed. The SEI layer forms on the electrode from the decomposition of electrolytes and solutes. A stable SEI layer passivates the electrode and mitigates dendrite formation, which could short-circuit the battery. Fan *et al.* [323] developed novel mixed electrolytes for LSB that enable the simultaneous formation of SEIs on both electrodes. Their SPAN-based LSBs with mixed electrolytes showed a high utilization of sulfur (over 80% at 0.15C), superior rate performance, excellent coulombic efficiency (≈100%), and long cycling life (1,000 cycles

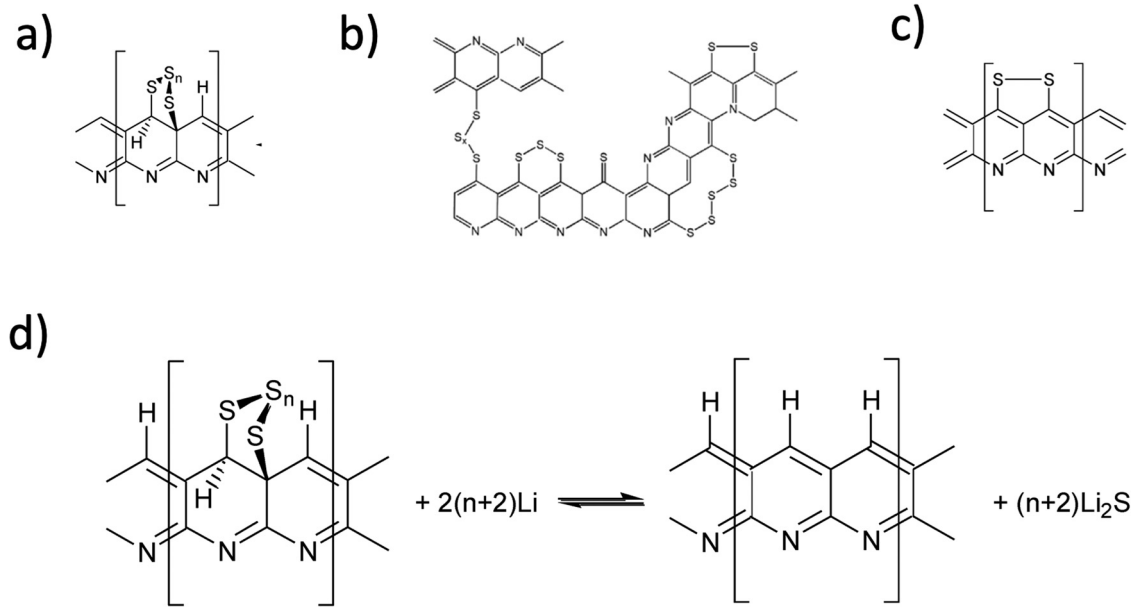

Figure 4: (a–c) Proposed chemical structures for SPAN based on pyrolysis temperature and duration [310]. (d) Lithiation of SPAN with the chemical structure shown in (a) does not result in the formation of higher-order polysulfides.

at 1C and 2,400 cycles at 7.5 C with capacity retention of 86.6 and 82.3%, respectively). Indeed, they were able to achieve high mass loadings and capacities as high as ~1,250 mA h/g at 0.75 C with no capacity fade up to 200 cycles. Liu *et al.* developed a gel polymer electrolyte, which showed stable performance even at high temperatures (55°C) compared to traditional liquid electrolytes [324]. A recently published mini-review about electrolyte regulation in lithium metal–SPAN battery can be found in ref. [325].

According to statistical analysis in ref. [253], 57% of >100 publications (in 2015–2016) reported areal sulfur loadings below 2 mg/cm and 49% corresponding areal capacities below 2 mA h/cm. Such electrodes are reasonable to use in reaction mechanism studies but unsuitable for practical application despite their high specific capacities (normalized by the amount of sulfur) because they deliver much lower gravimetric energy densities than commercial lithium-ion batteries [326]. An areal capacity of at least 6 mA h/cm is needed for LSBs to displace commercial LIBs because of the low operating voltage of LSBs (~2.1 V) [253]. Although there have been advances in the LSBs research, the commercialization is still lagging. This could be due to the fact that there is a vast difference on how research is conducted in academia and industry [327]. For example, usually coin cell is used in academia whereas pouch cell is generally used in industry. The advanced structures of the C/S that are used in academia are hard to produce in larger quantities [327]. Recently published article from Bhargav *et al.* have outlined some critical metrics, *viz.*, "Five 5s" (S-loading >5 mg/cm^2, C-content <5%, E/S ratio <5 µL/mg, N/P ratio <5, E/C ratio <5 µL/(mA h)) to achieve high energy density, which could be helpful to translate to industry [328]. Although "Five 5s" seems attractive, there are several issues that need to be addressed first. While increasing the loading might increase the energy density, it will adversely increase the electrochemical polarization, decrease the utilization and increase thermal instability [327,329,330].

Lastly, most studies report the gravimetric capacities of cathodes calculated based on the mass of sulfur. Unfortunately, although the sulfur content of some reported cathode materials can reach up to 70 wt%, the use of polymer binder (usually 10% of the slurry) and carbon black (usually ~10–20% of the slurry) in the slurry coating procedure (especially coating on the widely used aluminum foil current collector) results in a low-rate capacity on the electrode level in addition to a low gravimetric energy density [253]. High sulfur loading cathodes with high sulfur utilization and lightweight current collectors are essential for realizing high-energy-density LSBs. Recently, more efforts have been focused on self-supporting cathode electrodes [331–337]. Manthiram *et al.* [338] developed graphene-wrapped double-shelled hollow carbon sphere cathode with sulfur loading of 3.9 mg/cm^2, which exhibited a stable areal capacity of ~2 mA h/cm^2 at a current density of 3.3 mA/cm^2. Zheng *et al.* [339] fabricated a two-dimensional carbon yolk-shell nanosheets cathode

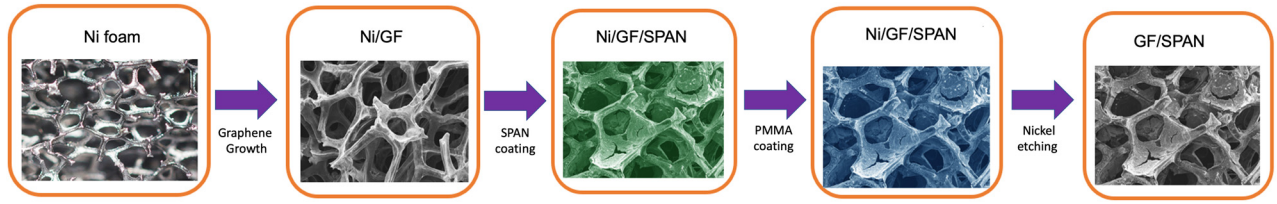

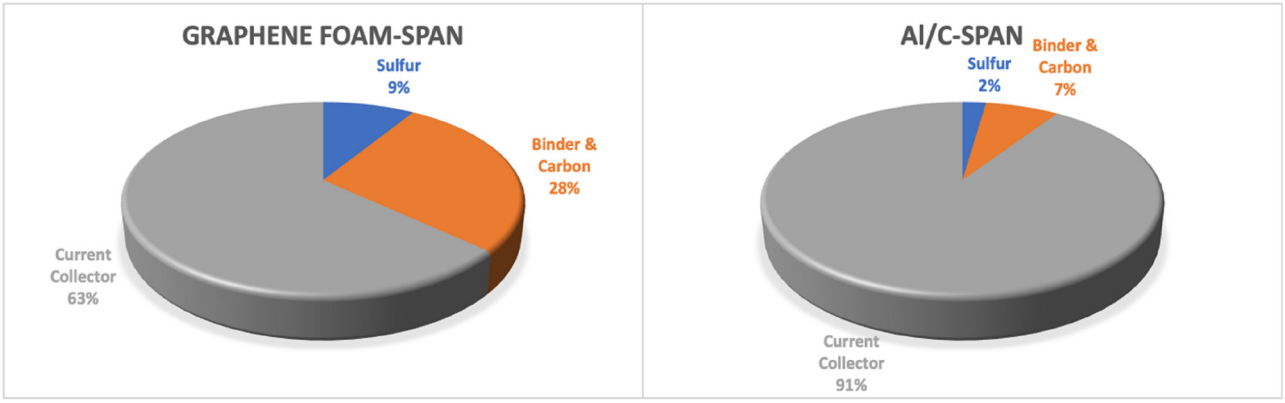

Figure 5: Top panel: A schematic showing the fabrication steps of a GF/SPAN cathode: GF is grown on a 3D-Ni mesh using the chemical vapor deposition technique. The GF/SPAN cathode electrode was prepared by vacuum filtrating a slurry of SPAN, carboxymethyl cellulose, and carbon black (mass ratio of 70:15:15) onto the GF current collector (with Ni mesh). The as-prepared cathode electrode was air-dried overnight followed by drying in an oven ~130°C for 12 h. Next, 5 wt% poly(methyl methacrylate) thin layer was coated on the cathode before it was submerged in a 6 M HCl solution for 6 h at 70°C to completely remove the nickel. The resulted cathode electrode was cleaned in KOH solution and washed in DI H_2O and dried [341]. Bottom panel: Weight comparison of different components inside the electrode for same S-loadings [341].

with sulfur loading of 10 mg/cm^2 that delivered an areal capacity of ~11.4 mA h/cm^2 after 50 cycles at a current density of 1.68 mA/cm^2. Lou *et al.* [300] designed a free-standing pie-like cathode by sulfurizing the electrospun PAN/polystyrene paper and wrapping the carbon–sulfur composite film with a thin layer of functionalized rGO. The pie-like cathode with a sulfur loading of 10.8 mg/cm^2 showed an areal capacity of ~10.7 mA h/cm^2 at a current density of 1.2 mA/cm^2. Liu *et al.* [335] developed a continuous core-shell structure of boron-doped carbon–sulfur aerogel (S-loading ~13.5 mg/cm^2) and achieved an areal capacity of 12.3 mA h/cm^2. Zhang *et al.* [332] showed dense monolithic metal-organic framework (MOF) and CNT can be used for sulfur electrode, which exhibited high areal (10.7 mA h/cm^2) and volumetric (676 mA h/mL) capacity. Sulfur can be infiltrated inside the VACNTs to get high areal capacity LSBs [331,340]. In this regard, we fabricated LSB cathodes by vacuum filtrating aqueous SPAN slurry through chemical vapor deposition grown free-standing graphene foam. More importantly, porous 3D graphene foams allowed S loadings as high as ~26 mg/cm^2 without any delamination or increased electrical resistance unlike Al foils that could only support a maximum S loading of 0.2–0.4 mg/cm^2 (Al–SPAN) without the binders (Figure 5). The graphene foam–SPAN (GF–SPAN) cathodes outperformed conventional Al–SPAN cathodes at the electrode level with areal capacity ~20 mA h/cm^2 at the current density of 3 mA/cm^2 (Table 8) [341].

4 Anodes

4.1 Li metal

Li metal is the ideal anode for LIBs due to its low density (0.59 g/cm^3) and negative electrochemical potential (–3.04 V) and high theoretical gravimetric capacity (3,860 mA h/g) [344,345]. Li-metal anodes are prone to dendrite formation, which can cause short circuits, thermal runaway reactions on the cathode, and could also cause the battery to catch fire. Indeed, in 1976, Exxon tried to commercialize Li metal batteries (anode Li metal, cathode TiS_2); however, the task was unsuccessful due to safety concerns that resulted from short circuiting [6,346]. Furthermore, Li-metal anodes also suffer from poor cycle life due to volume changes and subsequent formation of unstable SEI during cycling [345,347–353].

Table 8: Representative electrochemical performance of sulfur cathodes

Material	Operating voltage (V)	Initial/final capacity (mA h/g)	Cycle/C rate	Year/Ref.
Puffed rice derived carbon/Ni/S	1.7–2.8	1,257/821	500/0.2C	2018 [275]
Macro porous carbon nanotubes/S	1.5–2.8	1,544/901	100/0.5C	2018 [283]
Porous carbon fibers/vanadium nitride/S	1.7–2.8	1310.8/1052.5	250/0.1C	2018 [278]
N, O, and P-doped carbon/S	1.7–3.0	921/489	300/0.2C	2019 [287]
rGO–carbon composite–S paper	1.8–2.6	997/670	400/0.2C	2019 [298]
S/superP@SPAN	1.0–3.0	1,500/1,251	100/0.1C	2019 [322]
Porous SPAN fiber	1.0–3.0	903/903	150/1C	2019 [320]
Carbon–cotton/S	1.5–3.0	1,173/788	100/0.1C	2016 [301]
SPAN–carbon fiber current collector	1.0–3.5	1,640/1,250	100/NA	2017 [319]
Boron-doped carbon/S aerogel	1.8–3.0	1,120/836	500/1C	2019 [335]
Functionalized super aligned CNT/S	1.6–2.8	1,079/741	400/1C	2019 [334]
Dense monolithic MOF and CNT/S	1.5–3.0	580/470	300/1C	2019 [332]
Sulfur sandwiched between CeO_2–CNT@C membrane	1.7–2.8	1,300/847	100/0.2C	2020 [342]
S@$LiAlO_2$ on aluminum foil	1.8–2.6	989/842	100/0.2C	2020 [343]
Sulfur infused porous carbon	1.7–2.8	1,143/950	200/0.2C	2020 [336]
Graphene foam–SPAN	1.0–3.0	800/728	500/1C	2021 [341]

In the past 7 years, many research groups have been trying to revive the Li metal as a stable anode using different strategies such as optimization of solid/liquid electrolytes and additives [354–359], protective surface coatings (/artificial SEI layer) [353,360–363], modified separator [364,365], and the design of 3D conductive Li host [351,366–373]. Although such strategies improve the lifespan of the Li-metal anode, commercial applications of such batteries are still far away as they still have many disadvantages. Although surface coatings and solid electrolyte combination can increase the ionic concentration, it inevitably increases internal interfacial impedance that adversely affects the cycling stability [358,362,374]. Nanostructures such as MOFs [375], carbon materials [376,377], and 3D current collectors [375,378,379], which have pre-stored lithium, along with artificial SEI layer are promising alternatives [375]. This kind of structure can simultaneously address the volume change and unstable SEI formation. In this review, anodes beyond Li are discussed. A detailed review focused on Li-metal batteries can be found in refs [345,358]. Lastly, it should be noted that lithium-air batteries (specific energy ~5,200 W h/kg) wherein air is used as a cathode, have also been researched extensively in an effort to enhance the specific energy of the battery [380,381]. However, the practical application of such batteries is still far fetched due to the side reaction with electrolytes, poor cycling stability, and elimination of water and CO_2 [382]. The recent efforts that are focused on developing the electrolytes and porous cathode materials can be found in the review articles [380–383].

4.2 Intercalating anodes

Graphitic anodes (theoretical capacity ~372 mA h/g) initially enabled LIBs to become commercially viable and are still used widely due to their low cost and excellent stability [6]. In graphitic anodes, Li ions intercalate between the graphene planes, which offers good 2D mechanical stability, electrical conductivity, and Li^+ transport. Different forms of carbon such as graphite, CNTs, carbon fibers, exfoliated graphene, and rGO have been used as anodes [151]. The demand for new anode materials with higher capacity has increased as the theoretical limit of graphitic anodes has already been achieved commercially [384].

Titanium-based oxides (*e.g.*, LTO) also have received much attention despite having low intrinsic conductivity and low theoretical capacity (175 mA h/g) because they show low volume change (2–3%) upon Li insertion/de-insertion. Additionally, they also exhibit excellent cycling life [385–388]. LTO is relatively safer due to its high open-circuit voltage (~1.55 V), which prevents dendrite formation [384,389–392]. To improve the low intrinsic conductivity, similar approaches as in the case of the spinel layered cathodes have been suggested. For example, many strategies such as doping [393–396], change in size and morphology [397–399], and combining/coating with conducting carbon additives [392,400–403] either individually or in combination have been used (Table 9) [393,404–407].

Table 9: Representative electrochemical performance of Li metal anode and intercalating anode

Material	Operating voltage (V)	Initial/final capacity (mA h/g)	Cycle/C rate	Year/Ref.
LiF and Li–Al alloy protected layer–Li metal/LFP	0.01–4.2	120.4/94.2	300/3C	2020 [354]
Organophosphate-derived dual-layered Li metal/sulfur	1.7–2.7	800/735	100/1C	2020 [353]
Polyacrylic acid-coated Li/Cu matrix//LCO	3.0–4.2	127/103	1,000/2C	2020 [375]
Pure LTO	1.0–2.5	55.6/39.5	500/10C	2019 [402]
N-doped LTO/carbon	1.0–2.5	121.8/117.1	500/10C	2019 [402]
Mesoporous carbon/LTO nanoflakes	0.01–3.0	1,000/300	100/1C	2019 [403]
LTO microspheres@C	1.0–2.5	212/201	500/1C	2018 [392]
Al^{3+} and Mn^{4+} co-doped LTO/CNT	1.0–3.0	286.2/259.5	100/0.1C	2020 [393]
Necklace-type LTO/VACNT nanocomposites	1.0–2.5	170/165	500/10C	2016 [401]
Nanostructured LTO/crystallite size-7 nm	1.0–2.5	143/129	800/10C	2018 [408]

5 Alloying-type AMs for anodes

Based on their high specific capacity, low delithiation potential, low cost, and safety, alloying type materials such Sn, Ge, and Si have garnered much attention as promising candidates for anode [409,410]. Although gravimetric capacity (Sn: 994 mA h/g, Ge: 1,625 mA h/g, Si: 4,200 mA h/g) of these materials is different, their volumetric capacity (Sn: 7,216 mA h/cm^3, Ge: 8,645 mA h/cm^3, Si: 9,786 mA h/cm^3) is almost the same. These anode materials suffer from a volume change during cycling and most of the approaches to mitigate volume change are similar to those used for Si. In this review, we will focus on Si as recent reviews on Sn and Ge can be found in refs. [52,411], respectively.

Si has both the highest gravimetric capacity (4,200 mA h/g, $Li_{22}Si_5$) and volumetric capacity (9,786 mA h/cm^3) among the anode material candidates (see Figure 1b). The practical application of Si anodes is, however, impeded by its lower conductivity, large volume expansion upon lithiation (~400%) during first discharge, pulverization during subsequent cycling, delamination from current collector, and unstable SEI layer [52,409,412–414]. Companies such as Sila Nanotechnology, Advano, and NanoGraf are leading the commercialization efforts for Si anodes, but none of them penetrated the market with their Si anode-based batteries yet.

Several strategies have been suggested to overcome the challenges mentioned above (Figure 6). These include change in size/morphology of Si (nanotube, nanorods, nanowires, and porous particles) [52,415–420], coating/mixing with carbon/carbon composite [412,421–426], 3D Si host/conductive framework [427–432], and optimization of electrolyte, binders, and additives [433]. These strategies have also been combined with one another to get better electrochemical performance [422,423,434]. A detailed review of the design/optimization of electrolytes and binders can be found in ref. [433]. Also, limiting the discharge voltage and avoiding the re-crystallization voltage (>80 mV) can mitigate the pulverization issue to some extent [428].

The particle's ability to resist mechanical degradation increases with tailoring its size from the bulk to the nanometer scale. Many studies have suggested that the stress generation and subsequent cracking/fracture of the particle is size dependent [415–420]. Above 150 nm, Si particles are susceptible to fracture [419]. Although nanostructuring reduces pulverization issues, it also increases side reaction with electrolyte, internal resistance of the electrode, and agglomeration of NPs [433]. Also, the volumetric capacity of the NPs is often lower because of the low density.

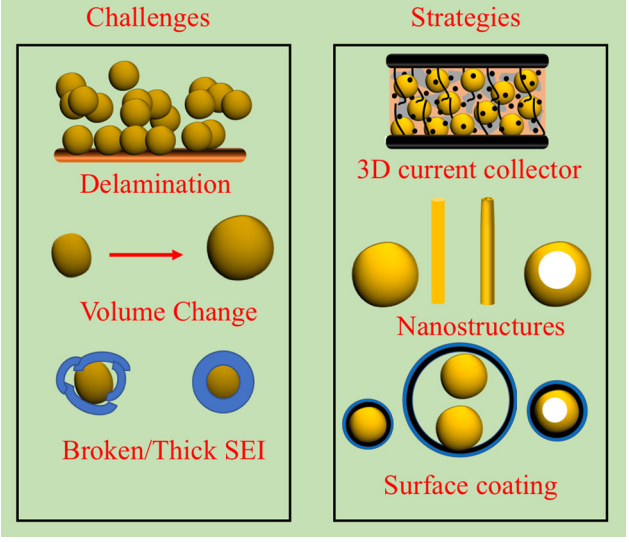

Figure 6: Schematic showing the challenges and strategies commonly found in the literature for Si anodes.

Nanostructures such as nanorods and nanowires were regarded as better alternatives; however, large capacity fading was observed in such structures due to an unstable SEI and delamination from the current collector [435,436]. Similar problems were observed with thin-film Si anodes with increasing thickness of the films [436]. Porous particles such as porous nanotubes and porous spheres can minimize the mechanical stress by providing the internal space for volumetric expansion and can shorten the Li-diffusion pathways [436,437]. Based on these findings, the development of innovative Si structures has gained momentum in recent years (Table 10) [438]. But, problems such as side reaction at the surface and growth of SEI still exist [437].

Carbon-based materials such as activated carbon, graphene, CNTs, and graphene oxide have been used to improve the conductivity of the electrode as well as the overall electrochemical activity of Si/C composite [409,439–442]. The electrochemical performance of such composite depends mostly upon the types of carbon matrix used. Pyrolytic carbon-coated Si NPs provide void space for volume change ensuing in excellent performance. Carbon coating can also reduce side reactions of electrolytes with Si and also prevent the growth of SEI [443–448]. Liu *et al.* [449] first showed the Si/C (yolk/shell) structure can be used. Subsequently, such C shells were replaced by other stable/porous metal/metal oxide as C cannot accommodate the volume change during long cycling [446,450]. 2D carbon forms such as graphene were also used to wrap SiNPs [422–425,439]. Luo *et al.* [421] showed that crumpled graphene/Si NPs have better cycle performance than bare Si NPs. Si/CNT have also shown promising performance [451,452]. Using CNTs alone may not be enough to mitigate volume change, and therefore CNTs are often used in conjunction with C [437,452]. A detailed review on surface coatings can be found in ref. [453].

Although several efforts have been made to accommodate volume changes by focusing on the AM alone, a key factor for the better electrode performance, that is, the current collector has been overlooked. Mostly, planar current collectors such as Cu-foils have been used in most studies. However, such Cu foil current collectors do not accommodate volume changes in the AM. However, 3D current collectors that can (i) provide better electrical connection between AM and CC reduce the CCAMI resistance, (ii) accommodate the volume change, and (iii) decrease the diffusion time are needed [428,434,454–456]. As an alternative approach to mixing Si NPs with other nanomaterials, we sandwiched SiNPs between freestanding CNT Bucky papers. This method alleviates the need for the traditional Cu current collector due to the high electrically conductive CNTs. Based on exhaustive electrochemical impedance spectroscopy studies, we found that the diffusion time constant for the sandwiched structures is ~150 times smaller than that of Cu foil [457].

6 CO_2 emissions

Although BEVs are touted as cleaner cars based on a comparison of their CO_2 emissions with respect to that

Table 10: Representative electrochemical performance of Si anode (1C = 4.2 A/g)

Material	Operating voltage (V)	Initial/final capacity (mA h/g)	Cycle/C rate	Year/Ref.
Micro-sized Si particle	0.001–1.5	2,100/275	20/0.25C	2019 [458]
Micro-sized branched Si particle	0.001–1.5	1,600/1,133	100/0.25C	2019 [458]
Si (<100 nm) NPs	0.01–1.2	193.2/68.5	100/0.05C	2019 [459]
Si (<100 nm)@mesoporous carbon	0.01–1.2	1,340/1,330	100/0.05C	2019 [459]
Si/CNT	0.001–2.0	1,537/246	100/0.25C	2018 [452]
Si/CNT/C microsphere	0.001–2.0	1,989/1,392	100/0.25C	2018 [452]
Double core-shell porous Si–Ag/C	0.01–1.5	1566.7/1,000	100/0.5C	2018 [450]
3D graphdiyne–Si	0.01–2.0	1,770/1,250	100/0.25C	2018 [430]
Si@N-doped carbon	0.01–2.0	2,385/2,003	500/0.2C	2020 [460]
Si@graphene	0.01–1.5	3,578/1,909	100/0.05C	2019 [461]
Hollow Si@void@C microspheres	0.01–1.5	3,000/1,040	500/0.5C	2019 [447]
Si@MOF derived C	0.005–3.0	2,709/1,978	350/0.25C	2020 [462]
MXene–Si–CNT	0.01–1.5	1,050/841	200/0.5C	2019 [463]
Si@CNT/C-microscroll	0.01–2.0	2,710/2,056	300/0.05C	2020 [464]
Amorphous Si@SiO_x thin film	0.01–1.0	2,173/2,116	100/0.5C	2019 [465]
Si – carbon coaxial nanotube as CC	0.05–1.0	2,750/2,200	50/0.2C	2011 [428]
Si – 3D Cu foil/Cu nanowires/CNT as CC	0.01–2.0	2,168/1,845	180/0.8C	2019 [434]
Bucky paper/Si/Bucky paper sandwich	0.01–1.0	2,900/1,635	100/0.1C	2020 [457]

of gasoline-powered vehicles, there are several factors ranging from mining/manufacturing to driving to disposal or recycling which might have a larger effect on the CO_2 emission from BEVs. Despite their low operation (driving) emissions, the CO_2 emission from the BEV manufacturing is more because of the added emissions during battery manufacturing, which is negligible during the manufacturing of gasoline-powered vehicles (pink bars in Figure 7a). Overall, present analyses suggest that mid-size BEVs will have a 51% reduction in CO_2 emission during operation compared to gasoline-powered vehicles (Figure 7a) [466]. In reality, this percent reduction is highly dependent on how the electricity used during manufacturing was produced. If the electricity grids were not cleaner and used non-renewable sources like coal, then the overall manufacturing CO_2 emissions are higher. Therefore, in our analysis of the overall emissions, a key factor that has been overlooked (gray bars in Figure 7a) and must be considered is whether or not clean energy was used during manufacturing. In addition, the battery chemistry also contributes to the CO_2 emission (Figure 7b). For mid-size BEV with LCO (hydrothermal process), the CO_2 emission is increased by ~45%, whereas for the LCO (solid-state process) the emission is increased by only ~9% [466]. If instead LMO is used, then the CO_2 emission will be decreased by ~18% and ~43% for mid-size and full-size BEVs, respectively (Table 11) [466,467].

In general, the total emissions (T_e) from an automobile could be expressed as a sum of emissions from manufacturing (E_m), operation (E_o), and disposal/recycling (E_d).

$$T_e(t) = E_m + E_o(t) + E_d. \quad (1)$$

In equation (1), T_e and E_o are time dependent as ~65% emissions of an automobile come from its operation over a period of time [466]. In the case of a BEV, the total manufacturing and disposal emissions contribute up to 30–35% of lifetime global warming emissions [466]. Thus, for BEVs, E_m could be decoupled into manufacturing emissions from batteries (E_{bm}) and emissions from other car parts and assembly (E_{cm}).

$$E_m = E_{bm} + E_{cm}. \quad (2)$$

In a typical mid- or full-size BEVs, E_{bm} contributes ~15–35% (for present-day LIBs) to E_m while E_{cm} contributes ~65–85%.

The offset in total emissions by using BEVs $\Delta T_e(t)$ in place of gasoline vehicles would be

$$\begin{aligned}\Delta T_e(t) &= (T_e)_{BEV} - (T_e)_{gasoline} \\ &= (E_{bm} - E_{gasoline}) + \Delta E_{cm} + \Delta E_o(t) + \Delta E_d.\end{aligned} \quad (3)$$

In equation (3), $(E_{bm} - E_{gasoline})$ is the difference between emissions for battery manufacturing and well-to-tank emissions for gasoline or diesel production. The total E_{bm} for LIBs ranges from 123 to 1,090 lbs of CO_2 per kW h [468] while $E_{gasoline}$ is 0.16 lbs per kW h of gasoline [469]. Given that well-to-tank emissions of gasoline are at least several magnitudes lower than battery emissions, we approximate $E_{bm} - E_{gasoline} \cong E_{bm}$. From the available data on BEV and gasoline car manufacturing [466], ΔE_{cm} could be neglected due to its minimal contribution

Table 11: Representative battery chemistry and global warming emission change. This table is obtained from ref. [466]

Battery	Process	Mid-size BEV (%)	Full-size BEV (%)
LCO	Solid state	9	−25
LFP	Solid state	−14	−41
LCO	Hydrothermal	45	NA
LFP	Hydrothermal	−7	−36
LMO	NA	−18	−43

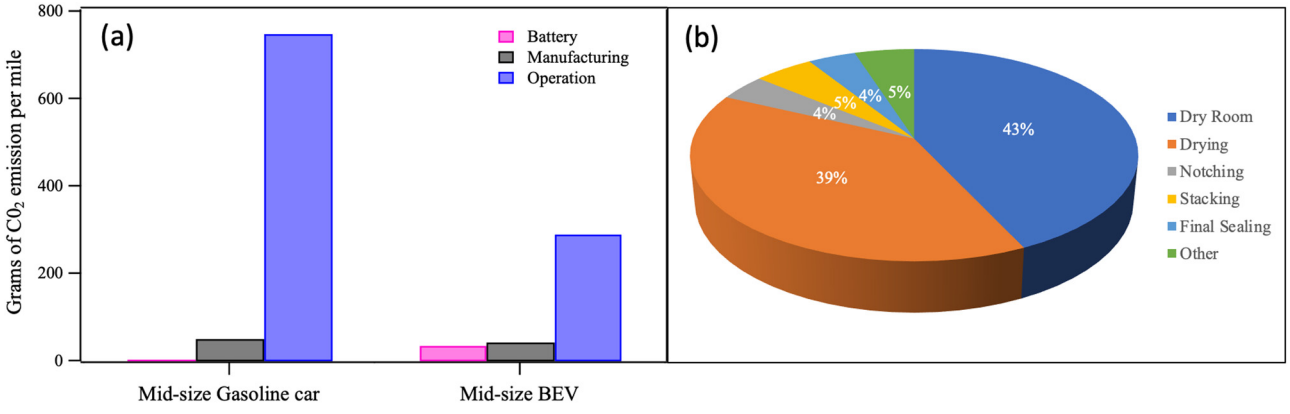

Figure 7: (a) Comparison of CO_2 emission from mid-size gasoline and BEV [466]. (b) Comparison between energy required during the assembly of battery when NMP is used as the solvent [467].

(*i.e.*, no significant difference in emissions from the car body parts such as tires and metal frame; see Figure 7a). The difference in emissions from battery disposal (ΔE_d) is significantly low (<5% of E_m for present-day LIBs). Thus, following the earlier approximations, we may express

$$\Delta T_e(t) \cong E_{bm} + \Delta E_o(t) \tag{4}$$

It is important to note that the term $\Delta E_o(t)$ is a highly dependent electricity grid mix representative of where BEVs are used. By explicitly including gasoline efficiency (e_{gas} in miles per gallon or mpg), BEV efficiency (e_{BEV} in miles per kW h), and electricity mix (C_{em}, lbs of CO_2 emitted per kW h of electricity produced), one obtains

$$\Delta E_o(t) = (E_o)_{BEV} - (E_o)_{gasoline} = \left(\frac{C_{em}(t)}{e_{BEV}} - \frac{20}{e_{gas}}\right) M_y t \tag{5}$$

In equation (5), M_y stands for average annual miles per car (~13,500 miles per year in the United States) and t is expressed in years. Factor 20 comes from the fact that one gallon of gasoline results in ~20 lbs of CO_2 emissions. We used lbs of CO_2 emission instead of traditional metric tons as $\Delta T_e(t)$ and $\Delta E_o(t)$ pertain to a single BEV/gasoline car. Here, we assumed constant automobile efficiency during the lifetime of a car. Using equation (5) and converting all time-dependence into miles driven (M_d), the total offset in emissions becomes

$$\Delta T_e(\text{miles}) = E_{bm} + \left(\frac{C_{em}}{e_{BEV}} - \frac{20}{e_{gas}}\right) M_d. \tag{6}$$

In equation (6), E_{bm} depends upon the size of the car. For example, for a mid-size 84-mile-range BEV (/full-size 265-mile-range BEV), manufacturing emissions are approximately 15% (/68%), or 1 ton or 2,000 lbs (/6 tons or 12,000 lbs) of CO_2 higher than those of a comparable conventional gasoline vehicle. Accordingly, considering that $E_{bm} > 0$, ΔT_e is offset (*i.e.*, $\Delta T_e = 0$) only after BEV is driven for M_{offset} miles, which is given by

$$M_{offset} = (E_{bm})\left(\frac{20}{e_{gas}} - \frac{C_{em}}{e_{BEV}}\right)^{-1}. \tag{7}$$

Clearly, M_{offset} directly depends upon emissions from battery manufacturing E_{bm} in addition to C_{em} and e_{gas}. As shown in Figure 8a, C_{em} and e_{gas} have changed significantly over the past three decades. Based on these estimates, it is expected that e_{gas} will reach 45 mpg by 2025 and 55 mpg by 2030 [470–472]. Similarly, the use of renewable energy resources decreased C_{em} significantly in the last decade (Figure 8b) [470–472]. A BEV using a 40 kW h battery has embedded emissions of ~5,000 lbs of CO_2 from battery manufacturing (at an industry average 122 lbs of CO_2 per kW h of battery [473] that are equivalent to the CO_2 emissions caused by driving a diesel car with 45 mpg for ~11,300 miles before the electric car even has driven one meter.

Building on the data from Figure 8, Figure 9a shows different ΔT_e for different scenarios of E_{bm} and e_{gas} for mid-size vehicles used in the United States. It can be noticed that different lines (corresponding to different E_{bm} and e_{gas} combinations) intersect the x-axis (corresponding to $\Delta T_e = 0$) at different points (*i.e.*, each line has a different M_{offset}). In Figure 9b, differences in M_{offset} for various scenarios with different E_{bm} and e_{gas} are shown. It is evident that the increase in M_{offset} is significantly impacted by increases in emissions from battery manufacturing. A 50% increase in battery manufacturing emissions (from the present estimate 2,000 lbs of CO_2 to 3,000 lbs) increases M_{offset} from ~5,000 to 7,500 miles while a 100% increase leads to a higher M_{offset} of 10,000 miles. In other words, as the emission from battery manufacturing increases, it takes longer BEV driving time to

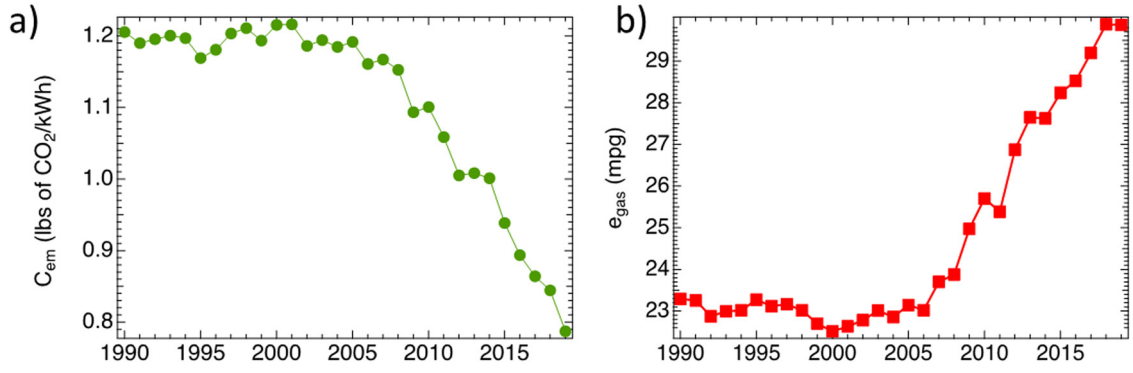

Figure 8: (a) Emissions per kW h of electricity produced in the United States and (b) increases in miles per gallon efficiency in internal combustion engine. For these calculations, the original data were taken from [470–472].

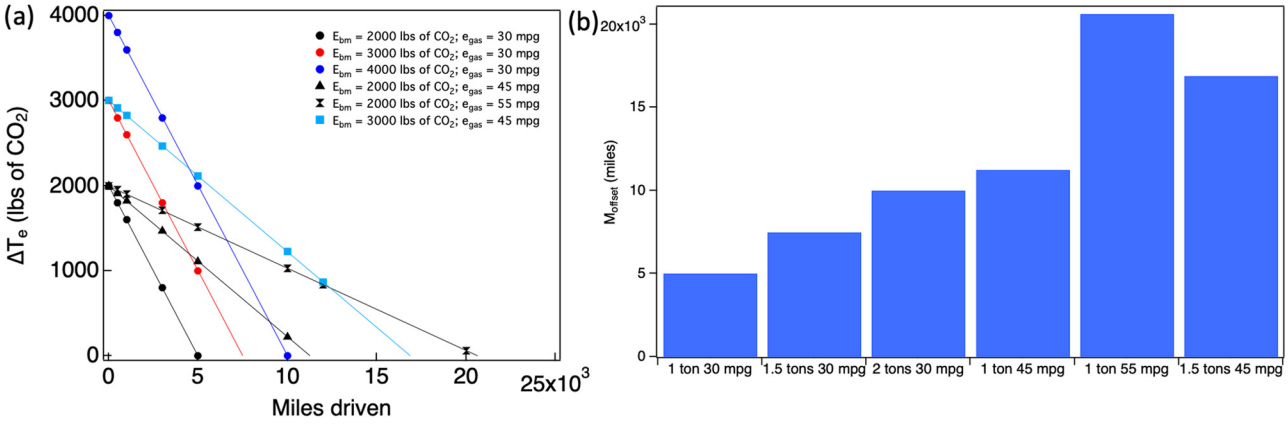

Figure 9: (a) The difference in total emissions (ΔT_e) between mid-size BEV and gasoline vehicles for different scenarios of battery manufacturing emissions (E_{bm}) and mileage (e_{gas}). Different scenarios require a different number of miles to be driven (M_{offset}) before total emissions could be offset ($\Delta T_e = 0$). (b) The values of M_{offse} for scenarios shown in (a). It should be noted that a conversion factor of 2,000 is used to convert lbs of CO_2 into tons.

offset the emissions (which is the primary goal of BEVs). More importantly, as seen from Figure 8b, e_{gas} increased non-linearly in the last two decades. Further expected increase in e_{gas} to 45 and 55 mpg for passenger vehicles (see Figure 9a and b) increases M_{offset} to ~11,250 and 20,650 miles, respectively. Lastly, in the developing world, C_{em} is much higher than the United States/Europe. For example, India (C_{em} = 1.63 lbs of CO_2 per kW h) and China (C_{em} = 1.35 lbs of CO_2 per kW h) have C_{em}, which is ~100% greater compared to the United States (~0.8 lbs of CO_2 per kW h) with lower average miles per year. In India, the average annual miles for a passenger car is ~7,500 miles much lower than the US value of ~13,500 miles. With combined effects of higher C_{em} and lower miles driven per year, a typical mid-size BEVs will take ~2 years (/3–4 years) to offset emissions that would have come from a gasoline car in the United States (/India). Given that C_{em} is dependent on geographical location, batteries produced in the developing world with higher C_{em} produce more E_{bm} per kW h [468].

The primary goal of road electrification is to offset CO_2 emissions from gasoline cars. While increasing power and energy density are necessary for ensuring that BEVs provide the same level of comfort as a gasoline car, newer battery chemistries should not significantly increase E_{bm}, E_{bd}, and M_{offset}. Concerted efforts have been focused on discovering new materials, novel architectures, and better chemistries (*e.g.*, Li–S batteries, Na–S batteries) with little or no attention paid to % increase in battery manufacturing emissions for new chemistries. Life cycle analyses (LCA) of present LIB-based BEV batteries suggest that significant emissions result from battery manufacturing. These emissions have been identified to directly depend upon the choice of cathode and anode materials in addition to other components [474–477]. For example, cathode material lithium NMC and anode material graphite together contribute 74% of the total carbon footprint of raw materials needed to make NCM LIBs [477]. Dunn *et al.* published a series of articles through Argonne National Labs with detailed LCA analysis for five LIB cathode materials [474–476]. Based on their analysis, for at-capacity battery assembly plants, battery materials dominate the carbon footprint of emissions, with cathode materials representing 10–50% of that energy, depending on cathode type. Similarly, based on the LIB LCA analysis from various publications presented in ref. [468], studies indicate that battery production is associated with significant emissions of up to 125 to 1,000 lbs of CO_2 per kW h for BEVs. In other words, a 24 kW h battery pack in Nissan Leaf results in E_{bm} = 2,480 lbs of CO_2 while a 100 kW h pack in Tesla Model S Long Range Plus leads to E_{bm} = 12,500 lbs of CO_2. As described in the mathematical framework earlier (*cf.* Figure 9), such high emissions imply that a higher M_{offset} (*i.e.*, significantly more miles need to be driven) is needed to offset ΔT_e.

Considering that the CO_2 emissions are dependent on materials chemistry (Table 11), current collectors, and manufacturing methods, we recommend that researchers use simple LCA based on existing battery chemistries (*e.g.*, GREET™ model from Argonne National Labs) to estimate % change in CO_2 emissions for any new active materials, composites, and electrode configurations (including changes in current collector or changes in manufacturing/assembly methods). For example, replacing traditional Al foil current collector with a nano-carbon matrix (*e.g.*, graphene foam, Bucky paper) could possibly lead to a significant increase in

CO_2 emissions in battery production based on the method used for graphene production (*e.g.*, chemical vapor deposition of graphene from CH_4 at 1,000°C produces significantly more emissions than exfoliation). In addition to complete electrochemical characterization, it is important for battery researchers to report % changes in CO_2 emissions per kW h that would be caused by their battery chemistry and assembly processes. Ignoring a net increase in CO_2 emissions for new materials or manufacturing processes while focusing exclusively on better electrochemical performance will eventually delay our efforts to mitigate the effects of climate change. Furthermore, one should also consider the recyclability of cell components, which ultimately could reduce the net CO_2 emissions at the materials production level.

7 Outlook and conclusions

Although AM chemical compositions and physical characteristics have been optimized, many studies are still focused on improving the gravimetric capacity of AMs and largely ignore the need to enhance areal capacity and volumetric capacity beyond existing commercial electrodes. Beyond these incremental studies, future research should also focus on improving the mass loading and tap density of the electrodes while maintaining a high areal capacity. It should be mentioned that there are important issues with how battery parameters are reported or compared in the literature. For example, (i) it is important to report gravimetric capacities at the electrode level and not just the AM level. Inactive binders and additives increase the total weight of the electrode and must be included in normalizing the total capacity to assess the practical usability of the electrodes and (ii) the C rate was developed to compare and evaluate similar electrodes that have similar cross-sectional area [478]. As a result, based on high gravimetric C rates obtained at the coin-cell level (with a small electrode area), it would be incorrect to claim that batteries in BEVs (with relatively higher electrode area) can be charged at a very high C rate within a few minutes. It is easy to maintain a high current density (a high C rate) in coin cells with a very small capacity per unit area for a short time. In larger cells, it may not be possible to maintain such high current densities for longer times because the Li^+ ion transport is limited by the diffusivity and the available cross-sectional area of the electrode. Furthermore, gravimetric C rates (calculated per gram of AM) should be converted to appropriate areal C rates (per cm^2 of the electrode) while assessing practical applications.

Although a lot of research has been focusing on alternative paper or carbon-based 2D/3D porous or nonporous electrodes, scaling up these techniques using current commercialized manufacturing systems is tricky. For example, to scale up from coin cells level to pouch cells, additional challenges such as gas evolution, placing tabs, or coating the slurry in a cost-effective manner must be addressed. A detailed discussion on gas evolution can be found in ref. [479]. While nano-structuring of AM has shown better results, most of the synthesis approaches reported in the literature are not cost effective because of the low product yield. For example, graphite is still used as the anode even though silicon has been known as an attractive alternative, and commercial silicon batteries remain implausible at this time. Several reports have appeared in the literature in which modified silicon (NPs, porous, core/shell) was used to obtain capacity as close as to its theoretical gravimetric capacity of 4,200 mA h/g. While such studies advance our understanding of battery chemistry, they fall short of commercializing the silicon battery technology. Replacing thermally and structurally stable layered oxides cathodes with sulfur-based cathodes pose a lot of challenges, mainly because of the lower open-circuit voltage (~2.1 V) in the latter that yields a lower energy density. Therefore, the areal capacity must be increased to 6 mA h/cm^2 by overcoming the insulating nature of sulfur and the polysulfide shuttle.

While this review is based on the experimental work reported in the literature, we also acknowledge the fact that extensive modeling of the electrochemical processes has helped advance LIBs [480,481]. Many approaches have been used to understand the electro-chemo mechanics [482], SEI formation [483], development of different components of the battery and its aging [484] as well as the safety [485,486]. Tools such as density functional theory (DFT) and molecular dynamics are used for computation and simulations for Li-ion batteries [323,480,487]. For example, Fan *et al.* [323] used DFT calculations to investigate the merit of using either ether-based or carbonate-based electrolyte solvents or a mixture of them in their LSBs. Specifically, they demonstrated that 1 M LiTFSI in $EC_{0.5}DME_{0.25}DOL_{0.25}$ yielded the best battery performance as the mixed electrolyte could promote the formation of a bilateral SEI. In this regard, machine learning is used extensively to identify optimal electrode materials, battery degradation patterns, state of charge, *etc.* [488–493]. As machine learning requires a significant amount of verified data as input, either experimental or computational data on hand or a combination of both is expected to accelerate new materials discovery for advanced LIBs. Additionally, in-depth knowledge of electrode materials and their electrochemical properties deduced from advanced *in situ*/operando tools constitutes

an important set of inputs for machine learning [494–496]. As such, *in situ*/*operando* characterization tools such as imaging (SEM, TEM, AFM), optical (Raman, UV/Vis, FTIR), X-ray, and neutron scattering have been extensively used in recent years. A detailed review on these techniques can be found in ref. [497]. Lastly, more importance must be given to explore environmentally friendly and facile routes that can displace the use of toxic solvents in nanomaterials synthesis and lithium battery manufacturing.

Funding information: This work was financially supported by NASA-EPSCoR award under #NNH17ZHA002C and South Carolina EPSCoR/IDeA Program under Award #18-SR03. The authors also thank all the members of Clemson Nanomaterials Institute for their inputs.

Author contributions: All authors have accepted responsibility for the entire content of this manuscript and approved its submission.

Conflict of interest: The authors state no conflict of interest.

References

[1] Omar N, Daowd M, van den Bossche P, Hegazy O, Smekens J, Coosemans T, et al. Rechargeable energy storage systems for plug-in hybrid electric vehicles – assessment of electrical characteristics. Energies. 2012;5:2952–88.

[2] Lu J, Chen Z, Ma Z, Pan F, Curtiss LA, Amine K. The role of nanotechnology in the development of battery materials for electric vehicles. Nat Nanotechnol. 2016;11:1031–8.

[3] Zaghib K, Mauger A, Groult H, Goodenough JB, Julien CM. Advanced electrodes for high power Li-ion batteries. Mater (Basel). 2013;6:1028–49.

[4] Brownson DAC, Kampouris DK, Banks CE. An overview of graphene in energy production and storage applications. J Power Sources. 2011;196:4873–85.

[5] Auston D, Samuelsen S, Brouwer J, DenBaars S, Glassley W, Jenkins B, et al. Chapter 5. assessing the need for high impact technology research, development & deployment for mitigating climate change. Collabra. 2016;2:1–24.

[6] Deng D. Li-ion batteries: basics, progress, and challenges. Energy Sci Eng. 2015;3:385–418.

[7] Cairns EJ, Albertus P. Batteries for electric and hybrid-electric vehicles. Annu Rev Chem Biomol Eng. 2010;1:299–320.

[8] Childress AS, Parajuli P, Zhu J, Podila R, Rao AM. A Raman spectroscopic study of graphene cathodes in high-performance aluminum ion batteries. Nano Energy. 2017;39:69–76.

[9] Lin MC, Gong M, Lu B, Wu Y, Wang DY, Guan M, et al. An ultrafast rechargeable aluminium-ion battery. Nature. 2015;520:325–8.

[10] Bommier C, Ji X. Electrolytes, SEI formation, and binders: a review of nonelectrode factors for sodium-ion battery anodes. Small. 2018;14:1703576.

[11] Wu C, Tong X, Ai Y, Liu DS, Yu P, Wu J, et al. The surface coating of commercial $LiFePO_4$ by utilizing ZIF-8 for high electrochemical performance lithium ion battery. Nano-Micro Lett. 2018;10:1–18.

[12] Zhang Y, Liang Q, Huang C, Gao P, Shu H, Zhang X, et al. Nearly monodispersed $LiFePO_4F$ nanospheres as cathode material for lithium ion batteries. J Solid State Electrochem. 2018;22:1995–2002.

[13] Liu Y, Sun Q, Li W, Adair KR, Li J, Sun X. A comprehensive review on recent progress in aluminum–air batteries. Green Energy Env. 2017;2:246–77.

[14] Zhang W, Mao J, Li S, Chen Z, Guo Z. Phosphorus-based alloy materials for advanced potassium-ion battery anode. J Am Chem Soc. 2017;139:3316–9.

[15] Meng YS, Arroyo-De Dompablo ME. Recent advances in first principles computational research of cathode materials for lithium-ion batteries. Acc Chem Res. 2013;46:1171–80.

[16] Islam MS, Fisher CAJ. Lithium and sodium battery cathode materials: computational insights into voltage, diffusion and nanostructural properties. Chem Soc Rev. 2014;43:185–204.

[17] Nitta N, Wu F, Lee JT, Yushin G. Li-ion battery materials: present and future. Mater Today. 2015;18:252–64.

[18] Whittingham MS, Gamble FR. The lithium intercalates of the transition metal dichalcogenides. Mater Res Bull. 1975;10:363–71.

[19] Mizushima K, Jones PC, Wiseman PJ, Goodenough JB. $LixCoO_2$ ($0 < x < -1$): a new cathode material for batteries of high energy density. Mater Res Bull. 1980;15:783–9.

[20] Jung YS, Cavanagh AS, Dillon AC, Groner MD, George SM, Lee S-H. Enhanced stability of $LiCoO_2$ cathodes in lithium-ion batteries using surface modification by atomic layer deposition. J Electrochem Soc. 2010;157:A75.

[21] Chen Z, Dahn JR. Methods to obtain excellent capacity retention in $LiCoO_2$ cycled to 4.5 V. Electrochim Acta. 2004;49:1079–90.

[22] Cho J, Kim YJ, Kim TJ, Park B. Zero-strain intercalation cathode for rechargeable Li-ion cell. Angew Chem - Int Ed. 2001;40:3367–9.

[23] MacNeil DD, Dahn JR. The reaction of charged cathodes with nonaqueous solvents and electrolytes: II. $LiMn_2O_4$ charged to 4.2 V. J Electrochem Soc. 2001;148:A1211.

[24] Ohzuku T. Electrochemistry and structural chemistry of $LiNiO_2$ (R3m) for 4 volt secondary lithium cells. J Electrochem Soc. 1993;140:1862–70.

[25] Rougier A, Gravereau P, Delmas C. Optimization of the composition of the $Li_{1-z}Ni_{1+z}O_2$ electrode materials: structural, magnetic, and electrochemical studies. J Electrochem Soc. 1996;143:1168–75.

[26] Arai H, Okada S, Sakurai Y, Yamaki JI. Thermal behavior of $Li_{1-y}NiO_2$ and the decomposition mechanism. Solid State Ion. 1998;109:295–302.

[27] Armstrong AR, Bruce PG. Synthesis of layered $LiMnO_2$ as an electrode for rechargeable lithium batteries. Nature. 1996;381:499–500.

[28] Davidson IJ, McMillan RS, Murray JJ, Greedan JE. Lithium-ion cell based on orthorhombic $LiMnO_2$. J Power Sources. 1995;54:232–5.

[29] Croguennec L, Deniard P, Brec R. Electrochemical cyclability of orthorhombic $LiMnO_2$: characterization of cycled materials. J Electrochem Soc. 1997;144:3323–30.

[30] Mishra SK, Ceder G. Structural stability of lithium manganese oxides. Phys Rev B - Condens Matter Mater Phys. 1999;59:6120–30.

[31] Fergus JW. Recent developments in cathode materials for lithium ion batteries. J Power Sources. 2010;195:939–54.

[32] Ammundsen B, Paulsen J. Novel lithium-ion cathode materials based on layered manganese oxides. Adv Mater. 2001;13:943–56.

[33] Capitaine F, Gravereau P, Delmas C. A new variety of $LiMnO_2$ with a layered structure. Solid State Ion. 1996;89:197–202.

[34] Chen CH, Liu J, Stoll ME, Henriksen G, Vissers DR, Amine K. Aluminum-doped lithium nickel cobalt oxide electrodes for high-power lithium-ion batteries. J Power Sources. 2004;128:278–85.

[35] Armstrong AR, Robertson AD, Bruce PG. Structural transformation on cycling layered $Li(Mn_{1-y}Coy)O_2$ cathode materials. Electrochim Acta. 1999;45:285–94.

[36] Ceder G, Mishra SK. The stability of orthorhombic and monoclinic-layered $LiMnO_2$. Electrochem Solid-State Lett. 1999;2:550–2.

[37] Kalyani P, Kalaiselvi N. Various aspects of $LiNiO_2$ chemistry: a review. Sci Technol Adv Mater. 2005;6:689–703.

[38] Armstrong AR, Robertson AD, Gitzendanner R, Bruce PG. The layered intercalation compounds $Li(Mn_{1-y}Coy)O_2$: positive electrode materials for lithium–ion batteries. J Solid State Chem. 1999;145:549–56.

[39] Ding Y, Cano ZP, Yu A, Lu J, Chen Z. Automotive Li-ion batteries: current status and future perspectives. Electrochem Energy Rev. 2019;2:1–28.

[40] Zhang R, Xia B, Li B, Lai Y, Zheng W, Wang H, et al. Study on the characteristics of a high capacity nickel manganese cobalt oxide (NMC) lithium-ion battery – an experimental investigation. Energies. 2018;11:2275.

[41] Zeng X, Zhan C, Lu J, Amine K. Stabilization of a high-capacity and high-power nickel-based cathode for Li-ion batteries. Chem. 2018;4:690–704.

[42] Chakraborty A, Kunnikuruvan S, Kumar S, Markovsky B, Aurbach D, Dixit M, et al. Layered cathode materials for lithium-ion batteries: review of computational studies on $LiNi_{1-x-y}Co_xMn_yO_2$ and $LiNi_{1-x-y}Co_xAlyO_2$. Chem Mater. 2020;32:915–52.

[43] Hua W, Zhang J, Zheng Z, Liu W, Peng X, Guo XD, et al. Na-doped Ni-rich $LiNi_{0.5}Co_{0.2}Mn_{0.3}O_2$cathode material with both high rate capability and high tap density for lithium ion batteries. Dalt Trans. 2014;43:14824–32.

[44] Dixit M, Markovsky B, Aurbach D, Major DT. Unraveling the effects of al doping on the electrochemical properties of $LiNi_{0.5}Co_{0.2}Mn_{0.3}O_2$ using first principles. J Electrochem Soc. 2017;164:A6359–65.

[45] Schipper F, Dixit M, Kovacheva D, Talianker M, Haik O, Grinblat J, et al. Stabilizing nickel-rich layered cathode materials by a high-charge cation doping strategy: zirconium-doped $LiNi_{0.6}Co_{0.2}Mn_{0.2}O_2$. J Mater Chem A. 2016;4:16073–84.

[46] Dixit M, Markovsky B, Schipper F, Aurbach D, Major DT. Origin of structural degradation during cycling and low thermal stability of Ni-rich layered transition metal-based electrode materials. J Phys Chem C. 2017;121:22628–36.

[47] Schipper F, Erickson EM, Erk C, Shin J-Y, Chesneau FF, Aurbach D. Review – recent advances and remaining challenges for lithium ion battery cathodes: I. nickel-rich, $LiNi_xCoyMnzO_2$. J Electrochem Soc. 2017;164:A6220–8.

[48] Ates MN, Jia Q, Shah A, Busnaina A, Mukerjee S, Abraham KM. Mitigation of layered to spinel conversion of a Li-rich layered metal oxide cathode material for Li-ion batteries. J Electrochem Soc. 2014;161:A290–301.

[49] Huang B, Li X, Wang Z, Guo H, Xiong X. Synthesis of Mg-doped $LiNi_{0.8}Co_{0.15}Al_{0.05}O_2$ oxide and its electrochemical behavior in high-voltage lithium-ion batteries. Ceram Int. 2014;40:13223–30.

[50] Yue P, Wang Z, Li X, Xiong X, Wang J, Wu X, et al. The enhanced electrochemical performance of $LiNi_{0.6}Co_{0.2}Mn_{0.2}O_2$ cathode materials by low temperature fluorine substitution. Electrochim Acta. 2013;95:112–8.

[51] Luo W, Zhou F, Zhao X, Lu Z, Li X, Dahn JR. Synthesis, characterization, and thermal stability of $LiNi_{1/3}Mn_{1/3}Co_{1/3-z}MgzO_2$, $LiNi_{1/3-z}Mn_{1/3}Co_{1/3}MgzO_2$, and $LiNi_{1/3}Mn_{1/3-z}Co_{1/3}MgzO_2$. Chem Mater. 2010;22:1164–72.

[52] Chen Y, Jiao Q, Wang L, Hu Y, Sun N, Shen Y, et al. Synthesis and characterization of $Li_{1.05}Co_{1/3}Ni_{1/3}Mn_{1/3}O_{1.95}X_{0.05}$ (X = Cl, Br) cathode materials for lithium-ion battery. Comptes Rendus Chim. 2013;16:845–9.

[53] Wan DY, Fan ZY, Dong YX, Baasanjav E, Jun HB, Jin B, et al. Effect of metal (Mn, Ti) doping on NCA cathode materials for lithium ion batteries. J Nanomater. 2018;2018:1–9.

[54] Wang D, Li X, Wang Z, Guo H, Xu Y, Fan Y, et al. Role of zirconium dopant on the structure and high voltage electrochemical performances of $LiNi_{0.5}Co_{0.2}Mn_{0.3}O_2$ cathode materials for lithium ion batteries. Electrochim Acta. 2016;188:48–56.

[55] Krishna Kumar S, Ghosh S, Ghosal P, Martha SK. Synergistic effect of 3D electrode architecture and fluorine doping of $Li_{1.2}Ni_{0.15}Mn_{0.55}Co_{0.1}O_2$ for high energy density lithium-ion batteries. J Power Sources. 2017;356:115–23.

[56] Krishna Kumar S, Ghosh S, Martha SK. Synergistic effect of magnesium and fluorine doping on the electrochemical performance of lithium-manganese rich (LMR)-based Ni-Mn-Co-oxide (NMC) cathodes for lithium-ion batteries. Ion (Kiel). 2017;23:1655–62.

[57] Nisar U, Amin R, Shakoor A, Essehli R, Al-Qaradawi S, Kahraman R, et al. Synthesis and electrochemical characterization of Cr-doped lithium-rich $Li_{1.2}Ni_{0.16}Mn_{0.56}Co_{0.08-x}CrxO_2$ cathodes. Emergent Mater. 2018;1:155–64.

[58] Liu S, Dang Z, Liu D, Zhang C, Huang T, Yu A. Comparative studies of zirconium doping and coating on $LiNi_{0.6}Co_{0.2}Mn_{0.2}O_2$ cathode material at elevated temperatures. J Power Sources. 2018;396:288–96.

[59] Eilers-Rethwisch M, Winter M, Schappacher FM. Synthesis, electrochemical investigation and structural analysis of doped $Li[Ni_{0.6}Mn_{0.2}Co_{0.2}\text{-}M]O_2$ (x = 0, 0.05; M = Al, Fe, Sn) cathode materials. J Power Sources. 2018;387:101–7.

[60] Pişkin B, Uygur CS, Aydınol MK. Morphology effect on electrochemical properties of doped (W and Mo) 622NMC, 111NMC, and 226NMC cathode materials. Int J Hydrog Energy. 2020;45:7874–80.

[61] Liu L, Sun K, Zhang N, Yang T. Improvement of high-voltage cycling behavior of $Li(Ni_{1/3}Co_{1/3}Mn_{1/3})O_2$ cathodes by Mg, Cr, and Al substitution. J Solid State Electrochem. 2009;13:1381–6.

[62] Kam KC, Mehta A, Heron JT, Doeff MM. Electrochemical and physical properties of Ti-substituted layered nickel manganese cobalt oxide (NMC) cathode materials. J Electrochem Soc. 2012;159:A1383–92.

[63] Zhang S, Ma J, Hu Z, Cui G, Chen L. Identifying and addressing critical challenges of high-voltage layered ternary oxide cathode materials. Chem Mater. 2019;31:6033–65.

[64] Chen M, Zhao E, Chen D, Wu M, Han S, Huang Q, et al. Decreasing Li/Ni disorder and improving the electrochemical performances of Ni-Rich $LiNi_{0.8}Co_{0.1}Mn_{0.1}O_2$by Ca doping. Inorg Chem. 2017;56:8355–62.

[65] Yang L, Ren F, Feng Q, Xu G, Li X, Li Y, et al. Effect of Cu doping on the structural and electrochemical performance of $LiNi_{1/3}Co_{1/3}Mn_{1/3}O_2$ cathode materials. J Electron Mater. 2018;47:3996–4002.

[66] Kim UH, Jun DW, Park KJ, Zhang Q, Kaghazchi P, Aurbach D, et al. Pushing the limit of layered transition metal oxide cathodes for high-energy density rechargeable Li ion batteries. Energy Env Sci. 2018;11:1271–9.

[67] Schipper F, Bouzaglo H, Dixit M, Erickson EM, Weigel T, Talianker M, et al. From surface ZrO_2 coating to bulk Zr doping by high temperature annealing of nickel-rich lithiated oxides and their enhanced electrochemical performance in lithium ion batteries. Adv Energy Mater. 2018;8:1701682.

[68] Sun Y, Zan L, Zhang Y. Enhanced electrochemical performances of Li_2MnO_3 cathode materials *via* adjusting oxygen vacancies content for lithium-ion batteries. Appl Surf Sci. 2019;483:270–7.

[69] Thackeray MM, Kang SH, Johnson CS, Vaughey JT, Benedek R, Hackney SA. Li_2MnO_3-stabilized $LiMO_2$ (M = Mn, Ni, Co) electrodes for lithium-ion batteries. J Mater Chem. 2007;17:3112–25.

[70] Zhang X, Xiong Y, Dong M, Hou Z. Pb-Doped lithium-rich cathode material for high energy density lithium-ion full batteries. J Electrochem Soc. 2019;166:A2960–65.

[71] Xie Q, Li W, Manthiram A. A Mg-doped high-nickel layered oxide cathode enabling safer, high-energy-density Li-ion batteries. Chem Mater. 2019;31:938–46.

[72] Torres-Castro L, Shojan J, Julien CM, Huq A, Dhital C, Paranthaman MP, et al. Synthesis, characterization and electrochemical performance of Al-substituted Li_2MnO_3. Mater Sci Eng B Solid-State Mater Adv Technol. 2015;201:13–22.

[73] Kim S, Noh JK, Yu S, Chang W, Chung KY, Cho BW. Effects of transition metal doping and surface treatment to improve the electrochemical performance of Li_2MnO_3. J Electroceram. 2013;30:159–65.

[74] Mori D, Sakaebe H, Shikano M, Kojitani H, Tatsumi K, Inaguma Y. Synthesis, phase relation and electrical and electrochemical properties of ruthenium-substituted Li_2MnO_3 as a novel cathode material. J Power Sources. 2011;196:6934–8.

[75] Xu Y, Cui Q. Nb-doped $Li_{1.20}[Mn_{0.54}Ni_{0.13}Co_{0.13}]O_2$ cathode material with enhanced electrochemical properties for lithium-ion battery. Int J Electrochem Sci. 2020;15:803–15.

[76] Wu ZL, Xie H, Li Y, Zhang F, Wang Z, Zheng W, et al. $Li_{1.2}Ni_{0.25}Mn_{0.55}O_2$: a high-capacity cathode material with a homogeneous monoclinic Li_2MnO_3-like superstructure. J Alloy Compd. 2020;827:154202.

[77] Zhao W, Oyama M, Yamada H, Noguchi H. Influence of Ti substitution on the structure and electrochemical properties of lithium-excess layered manganese based oxide for lithium ion batteries. Electrochim Acta. 2015;168:157–66.

[78] Yuge R, Kuroshima S, Toda A, Miyazaki T, Tabuchi M, Doumae K, et al. Structural and electrochemical properties of iron- and nickel-substituted Li_2MnO_3 cathodes in charged and discharged states. J Power Sources. 2017;365:117–25.

[79] Zhao W, Xiong L, Xu Y, Xiao X, Wang J, Ren Z. Magnesium substitution to improve the electrochemical performance of layered Li_2MnO_3 positive-electrode material. J Power Sources. 2016;330:37–44.

[80] Ma J, Zhou YN, Gao Y, Kong Q, Wang Z, Yang XQ, et al. Molybdenum substitution for improving the charge compensation and activity of Li_2MnO_3. Chem - A Eur J. 2014;20:8723–30.

[81] Gao Y, Wang X, Ma J, Wang Z, Chen L. Selecting substituent elements for Li-rich Mn-based cathode materials by density functional theory (DFT) calculations. Chem Mater. 2015;27:3456–61.

[82] Tabuchi M, Nabeshima Y, Takeuchi T, Kageyama H, Tatsumi K, Akimoto J, et al. Synthesis and electrochemical characterization of Fe and Ni substituted Li_2MnO_3 – an effective means to use Fe for constructing "Co-free" Li_2MnO_3 based positive electrode material. J Power Sources. 2011;196:3611–22.

[83] Cho J, Kim YW, Kim B, Lee JG, Park B. A breakthrough in the safety of lithium secondary batteries by coating the cathode material with $AlPO_4$ nanoparticles. Angew Chem - Int Ed. 2003;42:1618–21.

[84] Noh HJ, Youn S, Yoon CS, Sun YK. Comparison of the structural and electrochemical properties of layered Li[NixCoyMnz]O_2 (x = 1/3, 0.5, 0.6, 0.7, 0.8 and 0.85) cathode material for lithium-ion batteries. J Power Sources. 2013;233:121–30.

[85] Song C, Wang W, Peng H, Wang Y, Zhao C, Zhang H, et al. Improving the Electrochemical performance of $LiNi_{0.80}Co_{0.15}Al_{0.05}O_2$ in lithium ion batteries by $LiAlO_2$ surface modification. Appl Sci. 2018;8:378.

[86] Jung R, Metzger M, Maglia F, Stinner C, Gasteiger HAA. Oxygen release and its effect on the cycling stability of $LiNi_xMn_yCozO_2$(NMC) cathode materials for Li-ion batteries. J Electrochem Soc. 2017;164:A1361–77.

[87] Wang R, He X, He L, Wang F, Xiao R, Gu L, et al. Atomic structure of Li_2MnO_3after partial delithiation and Re-lithiation. Adv Energy Mater. 2013;3:1358–67.

[88] Thackeray MM, David WIF, Bruce PG, Goodenough JB. Lithium insertion into manganese spinels. Mater Res Bull. 1983;18:461–72.

[89] Xia Y, Zhou Y, Yoshio M. Capacity fading on cycling of 4VLi/$LiMn_2O_4$ Cells. J Electrochem Soc. 1997;144:2593–600.

[90] Aurbach D, Levi MD, Gamulski K, Markovsky B, Salitra G, Levi E, et al. Capacity fading of $LixMn_2O_4$ spinel electrodes studied by XRD and electroanalytical techniques. J Power Sources. 1999;81–82:472–9.

[91] Zhang C, Liu X, Su Q, Wu J, Huang T, Yu A. Enhancing electrochemical performance of $LiMn_2O_4$ cathode material at elevated temperature by uniform nanosized TiO_2 coating. ACS Sustain Chem Eng. 2017;5:640–7.
[92] Yao Y, Wang Z, Yu X, Zhang Y, Duan J, Zhu C, et al. Interface control strategy of synthesis $LiMn_2O_4@Al_2O_3$ assisted by tert-butanol. Int J Electrochem Sci. 2019;14:6478–87.
[93] Liu Y, Lin XJ, Sun YG, Xu YS, Chang BB, Liu CT, et al. Precise surface engineering of cathode materials for improved stability of lithium-ion batteries. Small. 2019;15:1901019.
[94] Wang S, Luo C, Feng Y, Fan G, Feng L, Ren M, et al. Electrochemical properties and microstructures of $LiMn_2O_4$ cathodes coated with aluminum zirconium coupling agents. Ceram Int. 2020;46:13003–13.
[95] Feng X, Zhang J, Yin L. Enhanced cycling stability of $Co_3(PO_4)_2$-coated $LiMn_2O_4$ cathode materials for lithium ion batteries. Powder Technol. 2016;287:77–81.
[96] Tron A, Park YD, Mun J. AlF_3-coated $LiMn_2O_4$ as cathode material for aqueous rechargeable lithium battery with improved cycling stability. J Power Sources. 2016;325:360–4.
[97] Hai Y, Zhang Z, Liu H, Liao L, Fan P, Wu Y, et al. Facile controlled synthesis of spinel $LiMn_2O_4$ porous microspheres as cathode material for lithium ion batteries. Front Chem. 2019;7:437.
[98] Zhu C. Novel fabrication of $Li_4Ti_5O_{12}$ coated $LiMn_2O_4$ nanorods as cathode materials with long-term cyclic stability at high ambient temperature. Int J Electrochem Sci. 2019;14:7673–83.
[99] Li S, Zhu K, Zhao D, Zhao Q, Zhang N. Porous $LiMn_2O_4$ with Al_2O_3 coating as high-performance positive materials. Ion (Kiel). 2019;25:1991–8.
[100] Liu S, Ni D, Li HF, Hui KN, Ouyang CY, Jun SC. Effect of cation substitution on the pseudocapacitive performance of spinel cobaltite MCo_2O_4(M = Mn, Ni, Cu, and Co). J Mater Chem A. 2018;6:10674–85.
[101] Michalska M, Ziółkowska DA, Jasiński JB, Lee PH, Ławniczak P, Andrzejewski B, et al. Improved electrochemical performance of $LiMn_2O_4$ cathode material by Ce doping. Electrochim Acta. 2018;276:37–46.
[102] Chen B, Ben L, Yu H, Chen Y, Huang X. Understanding surface structural stabilization of the high-temperature and high-voltage cycling performance of Al^{3+}-modified $LiMn_2O_4$ cathode material. ACS Appl Mater Interfaces. 2018;10:550–9.
[103] Yang Z, Wang Y, Chen X, Wu H, Zhang Y. $Mg^{2+}$and Ti^{4+}Co-doped spinel $LiMn_2O_4$ as lithium-ion battery cathode. ChemistrySelect. 2019;4:9583–9.
[104] Cai Z, Ma Y, Huang X, Yan X, Yu Z, Zhang S, et al. High electrochemical stability Al-doped spinel $LiMn_2O_4$ cathode material for Li-ion batteries. J Energy Storage. 2020;27:101036.
[105] Talyosef Y, Markovsky B, Lavi R, Salitra G, Aurbach D, Kovacheva D, et al. Comparing the behavior of nano- and microsized particles of $LiMn_{1.5}Ni_{0.5}O_4$ spinel as cathode materials for Li-ion batteries. J Electrochem Soc. 2007;154:A682.
[106] Sun Y, Yang Y, Zhan H, Shao H, Zhou Y. Synthesis of high power type $LiMn_{1.5}Ni_{0.5}O_4$ by optimizing its preparation conditions. J Power Sources. 2010;195:4322–6.
[107] Rapulenyane N, Ferg E, Luo H. High-performance $Li_{1.2}Mn_{0.6}Ni_{0.2}O_2$ cathode materials prepared through a facile one-pot co-precipitation process for lithium ion batteries. J Alloy Compd. 2018;762:272–81.
[108] Zhu Q, Zheng S, Lu X, Wan Y, Chen Q, Yang J, et al. Improved cycle performance of $LiMn_2O_4$ cathode material for aqueous rechargeable lithium battery by LaF_3 coating. J Alloy Compd. 2016;654:384–91.
[109] Padhi AK, Nanjundaswamy KS, Goodenough JB. Phospho-olivines as positive-electrode materials for rechargeable lithium batteries. J Electrochem Soc. 1997;144:1188–94.
[110] Nytén A, Abouimrane A, Armand M, Gustafsson T, Thomas JO. Electrochemical performance of Li_2FeSiO_4 as a new Li-battery cathode material. Electrochem commun. 2005;7:156–60.
[111] Zaghib K, Mauger A, Julien CM. Green energy and technology. Green Energy Technol. 2015;172:25–65.
[112] Li Z, Ren X, Zheng Y, Tian W, An L, Sun J, et al. Effect of Ti doping on $LiFePO_4$/C cathode material with enhanced low-temperature electrochemical performance. Ion (Kiel). 2020;26:1599–609.
[113] Göktepe H, Şahan H, Patat Ş. Effect of silver and carbon double coating on the electrochemical performance of $LiFePO_4$ cathode material for lithium ion batteries. Int J Hydrog Energy. 2016;41:9774–9.
[114] Liu Y, Manuel J, Zhao X, Haridas AK, Chauhan GS, Kim JK, et al. Effect of carbon coating and magnesium doping on electrochemical properties of $LiFePO_4$ for lithium ion batteries. Sci Adv Mater. 2017;9:1266–71.
[115] Li Y, Wang J, Huang HX, Wang J, Zhang M, Liang MmM. Co-coating effect of $GdPO_4$ and carbon on $LiFePO_4$ cathode surface for lithium ion batteries. Adv Powder Technol. 2019;30:1442–9.
[116] Ventrapragada LK, Zhu J, Creager SE, Rao AM, Podila R. A versatile carbon nanotube-based scalable approach for improving interfaces in Li-ion battery electrodes. ACS Omega. 2018;3:4502–8.
[117] Wang C, Li S, Han Y, Lu Z. Assembly of $LiMnPO_4$ nanoplates into microclusters as a high-performance cathode in lithium-ion batteries. ACS Appl Mater Interfaces. 2017;9:27618–24.
[118] Kim S-W, Kim J, Gwon H, Kang K. Phase stability study of $Li_{1-x}MnPO_4$ ($0 \leq x \leq 1$) cathode for Li rechargeable battery. J Electrochem Soc. 2009;156:A635.
[119] Satyavani TVSL, Srinivas Kumar A, Subba Rao PSV. Methods of synthesis and performance improvement of lithium iron phosphate for high rate Li-ion batteries: a review. Eng Sci Technol an Int J. 2016;19:178–88.
[120] Zhang J, Luo S, Wang Q, Wang Z, Zhang Y, Hao A, et al. Yttrium substituting in Mn site to improve electrochemical kinetics activity of sol-gel synthesized $LiMnPO_4$/C as cathode for lithium ion battery. J Solid State Electrochem. 2017;21:3189–94.
[121] Huang QY, Wu Z, Su J, Long YF, Lv XY, Wen YX. Synthesis and electrochemical performance of Ti–Fe co-doped $LiMnPO_4$/C as cathode material for lithium-ion batteries. Ceram Int. 2016;42:11348–54.
[122] Sarkar T, Bharadwaj MD, Waghmare UV, Kumar P. Mechanism of charge transfer in olivine-type $LiFeSiO_4$and $LiFe_{0.5}M_{0.5}SiO_4$(M = Mg or Al) cathode materials: first-principles analysis. J Phys Chem C. 2015;119:9125–33.
[123] Islam MS, Dominko R, Masquelier C, Sirisopanaporn C, Armstrong AR, Bruce PG. Silicate cathodes for lithium

batteries: alternatives to phosphates. J Mater Chem. 2011;21:9811–8.
[124] Arroyo-de Dompablo ME, Armand M, Tarascon JM, Amador U. On-demand design of polyoxianionic cathode materials based on electronegativity correlations: an exploration of the Li_2MSiO_4 system (M = Fe, Mn, Co, Ni). Electrochem commun. 2006;8:1292–8.
[125] Arthur Z, Chiu HC, Lu X, Chen N, Emond V, Zaghib K, et al. Spontaneous reaction between an uncharged lithium iron silicate cathode and a $LiPF_6$-based electrolyte. Chem Commun. 2016;52:190–3.
[126] Wang C, Xu Y, Sun X, Zhang B, Chen Y, He S. Enhanced electrochemical properties of F-doped Li_2MnSiO_4/C for lithium ion batteries. J Power Sources. 2018;378:345–52.
[127] Li YX, Gong ZL, Yang Y. Synthesis and characterization of Li_2MnSiO_4/C nanocomposite cathode material for lithium ion batteries. J Power Sources. 2007;174:528–32.
[128] Wang M, Yang M, Ma L, Shen X, Zhang X. Graphene channel liquid container field effect transistor as pH sensor. J Nanomater. 2014;2014:1–6.
[129] Fan XY, Li Y, Wang JJ, Gou L, Zhao P, Li DL, et al. Synthesis and electrochemical performance of porous Li_2FeSiO_4/C cathode material for long-life lithium-ion batteries. J Alloy Compd. 2010;493:77–80.
[130] Wang M, Ding C, Miao Y, Liu T, Hang K, Zhang J. Improving electrochemical properties and structural stability of lithium manganese silicates as cathode materials for lithium ion batteries *via* introducing lithium excess. Int J Energy Res. 2020;44:902–12.
[131] Hou P, Feng J, Wang Y, Wang L, Li S, Yang L, et al. Study on the properties of Li_2MnSiO_4 as cathode material for lithium-ion batteries by sol-gel method. Ion (Kiel). 2020;26:1611–6.
[132] Lv X, Zhao X, Wu S, Nguyen MC, Zhu Z, Lin Z, et al. Fe–Si networks and charge/discharge-induced phase transitions in Li_2FeSiO_4 cathode materials. Phys Chem Chem Phys. 2018;20:14557–63.
[133] Fedotov SS, Khasanova NR, Samarin AS, Drozhzhin OA, Batuk D, Karakulina OM, et al. $AVPO_4F$ (A = Li, K): a 4 V cathode material for high-power rechargeable batteries. Chem Mater. 2016;28:411–5.
[134] Kitajou A, Ishado Y, Inoishi A, Okada S. Amorphous xLiF-$FeSO_4$ ($1 \le x \le 2$) composites as a cathode material for lithium ion batteries. Solid State Ion. 2018;326:48–51.
[135] Kim M, Lee S, Kang B. Fast-rate capable electrode material with higher energy density than $LiFePO_4$: 4.2V $LiVPO_4F$ synthesized by scalable single-step solid-state reaction. Adv Sci. 2015;3:1500366.
[136] Harrison KL, Manthiram A. Microwave-assisted solvothermal synthesis and characterization of various polymorphs of $LiVOPO_4$. Chem Mater. 2013;25:1751–60.
[137] Kim M, Lee S, Kang B. High energy density polyanion electrode material: $LiVPO_4O_{1-x}F_x$($x \approx 0.25$) with tavorite structure. Chem Mater. 2017;29:4690–9.
[138] Zhang Y, Lv T, Gao P, Shu H, Yang X, Liang Q, et al. Ag nanoparticles promoted $LiFePO_4F$ nanospheres cathode with superior cycling stability for lithium-ion batteries. J Alloy Compd. 2018;751:12–9.
[139] Wu J, Xu Y, Sun X, Wang C, Zhang B, Zhao J. The multiple effects of potassium doping on $LiVPO_4F$/C composite cathode material for lithium ion batteries. J Power Sources. 2018;396:155–63.
[140] Zhang Y, Huo QY, Du PP, Wang LZ, Zhang AQ, Song YH, et al. Advances in new cathode material $LiFePO_4$ for lithium-ion batteries. Synth Met. 2012;162:1315–26.
[141] Adib M, Habib N, Ashry A, Fathalla M. On the use of silicon as thermal neutron filter. Ann Nucl Energy. 2003;30:1905–17.
[142] Yuan LX, Wang ZH, Zhang WX, Hu XL, Chen JT, Huang YH, et al. Development and challenges of $LiFePO_4$cathode material for lithium-ion batteries. Energy Env Sci. 2011;4:269–84.
[143] Chikkannanavar SB, Bernardi DM, Liu L. A review of blended cathode materials for use in Li-ion batteries. J Power Sources. 2014;248:91–100.
[144] Tan H, Xu L, Geng H, Rui X, Li C, Huang S. Nanostructured $Li_3V_2(PO_4)_3$Cathodes. Small. 2018;14:1800567.
[145] Vu A, Stein A. Lithium iron phosphate spheres as cathode materials for high power lithium ion batteries. J Power Sources. 2014;245:48–58.
[146] Qin X, Wang X, Xie J, Wen L. Hierarchically porous and conductive $LiFePO_4$ bulk electrode: binder-free and ultrahigh volumetric capacity Li-ion cathode. J Mater Chem. 2011;21:12444.
[147] Liu Y, Liu D, Zhang Q, Yu D, Liu J, Cao G. Lithium iron phosphate/carbon nanocomposite film cathodes for high energy lithium ion batteries. Electrochim Acta. 2011;56:2559–65.
[148] Wu XL, Guo YG, Su J, Xiong JW, Zhang YL, Wan LJ. Carbon-nanotube-decorated nano-$LiFePO_4$@C cathode material with superior high-rate and low-temperature performances for lithium-ion batteries. Adv Energy Mater. 2013;3:1155–60.
[149] Liu C, Li F, Lai-Peng M, Cheng HM. Advanced materials for energy storage. Adv Mater. 2010;22:E28–62.
[150] Xing Y, He YB, Li B, Chu X, Chen H, Ma J, et al. $LiFePO_4$/C composite with 3D carbon conductive network for rechargeable lithium ion batteries. Electrochim Acta. 2013;109:512–8.
[151] Goriparti S, Miele E, De Angelis F, Di Fabrizio E, Zaccaria RP, Capiglia C. Review on recent progress of nanostructured anode materials for Li-ion batteries. J Power Sources. 2014;257:421–43.
[152] Chen R, Zhao T, Zhang X, Li L, Wu F. Advanced cathode materials for lithium-ion batteries using nanoarchitectonics. Nanoscale Horiz. 2016;1:423–44.
[153] Liu HK, Wang GX, Guo Z, Wang J, Konstantinov K. Nanomaterials for lithium-ion rechargeable batteries. J Nanosci Nanotechnol. 2006;6(1):1–15.
[154] Ye SH, Lv JY, Gao XP, Wu F, Song DY. Synthesis and electrochemical properties of $LiMn_2O_4$ spinel phase with nanostructure. Electrochim Acta. 2004;49:1623–8.
[155] Uddin MJ, Alaboina PK, Cho SJ. Nanostructured cathode materials synthesis for lithium-ion batteries. Mater Today Energy. 2017;5:138–57.
[156] Okubo M, Hosono E, Kim J, Enomoto M, Kojima N, Kudo T, et al. Nanosize effect on high-rate Li-ion intercalation in $LiCoO_2$ electrode. J Am Chem Soc. 2007;129:7444–52.
[157] Zhang H, Xu Y, Liu D. Novel nanostructured $LiMn_2O_4$ microspheres for high power Li-ion batteries. RSC Adv. 2015;5:11091–95.
[158] Cai Y, Huang Y, Wang X, Jia D, Tang X. Long cycle life, high rate capability of truncated octahedral $LiMn_2O_4$ cathode materials synthesized by a solid-state combustion reaction for lithium ion batteries. Ceram Int. 2014;40:14039–43.

[159] Li S, Zhu K, Liu J, Zhao D, Cui X. Porous $LiMn_2O_4$ microspheres with different pore size: preparation and application as cathode materials for lithium ion batteries. J Electrochem Energy Convers Storage. 2019;16. doi: 10.1115/1.4040567.
[160] Li B, Wei X, Chang Z, Chen X, Yuan XZ, Wang H. Facile fabrication of $LiMn_2O_4$ microspheres from multi-shell MnO_2 for high-performance lithium-ion batteries. Mater Lett. 2014;135:75–8.
[161] Yang J, Guo B, He H, Li Y, Song C, Liu G. $LiNi_{0.5}Mn_{0.5}O_2$ hierarchical nanorods as high-capacity cathode materials for Li-ion batteries. J Alloy Compd. 2017;698:714–8.
[162] Pei Y, Chen Q, Xu CY, Wang HX, Fang HT, Zhou C, et al. Chelate-induced formation of Li_2MnSiO_4nanorods as a high capacity cathode material for Li-ion batteries. J Mater Chem A. 2016;4:9447–54.
[163] Li J, Hua Luo S, Wang Q, Yan S, Feng J, Liu H, et al. Facile synthesis of carbon-$LiMnPO_4$ nanorods with hierarchical architecture as a cathode for high-performance Li-ion batteries. Electrochim Acta. 2018;289:415–21.
[164] McNulty D, Buckley DN, O'Dwyer C. V_2O_3 polycrystalline nanorod cathode materials for Li-ion batteries with long cycle life and high capacity retention. ChemElectroChem. 2017;4:2037–44.
[165] Zhao H, Wang J, Wang G, Liu S, Tan M, Liu X, et al. Facile synthesis of orthorhombic $LiMnO_2$ nanorods by *in-situ* carbothermal reduction: promising cathode material for Li ion batteries. Ceram Int. 2017;43:10585–89.
[166] Bao L, Xu G, Sun X, Zeng H, Zhao R, Yang X, et al. Monodispersed $LiFePO_4$@C core-shell [001] nanorods for a high power Li-ion battery cathode. J Alloy Compd. 2017;708:685–93.
[167] Yang F, Zhang Q, Hu X, Peng T, Liu J. Preparation of Li-rich layered-layered type *x* $Li_2MnO_{3(1-x)}LiMnO_2$ nanorods and its electrochemical performance as cathode material for Li-ion battery. J Power Sources. 2017;353:323–32.
[168] Wang C, Cao Y, Luo Z, Li G, Xu W, Xiong C, et al. Flexible potassium vanadate nanowires on Ti fabric as a binder-free cathode for high-performance advanced lithium-ion battery. Chem Eng J. 2017;307:382–8.
[169] Hua K, Li X, Fang D, Bao R, Yi J, Luo Z, et al. Vanadium trioxide nanowire arrays as a cathode material for lithium-ion battery. Ceram Int. 2018;44:11307–13.
[170] Su D, Zhao Y, Yan D, Ding C, Ning M, Zhang J, et al. Enhanced composites of V_2O_5 nanowires decorating on graphene layers as ideal cathode materials for lithium-ion batteries. J Alloy Compd. 2017;695:2974–80.
[171] Deng B, Chen Y, Wu P, Han J, Li Y, Zheng H, et al. Lithium-rich layered oxide nanowires bearing porous structures and spinel domains as cathode materials for lithium-ion batteries. J Power Sources. 2019;418:122–9.
[172] Salvatierra RV, Raji ARO, Lee SK, Ji Y, Li L, Tour JM. Silicon nanowires and lithium cobalt oxide nanowires in graphene nanoribbon papers for full lithium ion battery. Adv Energy Mater. 2016;6:1600918.
[173] Bai N, Xiang K, Zhou W, Lu H, Zhao X, Chen H. $LiFePO_4$/carbon nanowires with 3D nano-network structure as potential high performance cathode for lithium ion batteries. Electrochim Acta. 2016;191:23–8.
[174] Zhu QP, Wang X, Fan J, Xu Q, Min Y. MnO_2 nanowires as precursor synthesis of lithium-rich cathode material with enhanced electrochemical performances. Ion (Kiel). 2019;25:2477–85.
[175] Zhang LX, Wang YZ, Jiu HF, Wang YL, Sun YX, Li Z. Controllable synthesis of Co-doped spinel $LiMn_2O_4$ nanotubes as cathodes for Li-ion batteries. Electron Mater Lett. 2014;10:439–44.
[176] Ding YL, Xie J, Cao GS, Zhu TJ, Yu HM, Zhao XB. Single-crystalline $LiMn_2O_4$ nanotubes synthesized *via* template-engaged reaction as cathodes for high-power lithium ion batteries. Adv Funct Mater. 2011;21:348–55.
[177] Ma D, Li Y, Zhang P, Cooper AJ, Abdelkader AM, Ren X, et al. Mesoporous $Li_{1.2}Mn_{0.54}Ni_{0.13}Co_{0.13}O_2$ nanotubes for high-performance cathodes in Li-ion batteries. J Power Sources. 2016;311:35–41.
[178] Da F, Que Yu,LF, Wang ZB, Zhang Y, Xue Y, Liu BS, et al. Layered-spinel capped nanotube assembled 3D Li-rich hierarchitectures for high performance Li-ion battery cathodes. J Mater Chem A. 2016;4:18416–25.
[179] Fang L, Zhang H, Zhang Y, Liu L, Wang Y. Design and synthesis of two-dimensional porous Fe-doped $LiCoPO_4$ nanoplates as improved cathode for lithium ion batteries. J Power Sources. 2016;312:101–8.
[180] Sun W, Cao F, Liu Y, Zhao X, Liu X, Yuan J. Nanoporous $LiMn_2O_4$ nanosheets with exposed {111} facets as cathodes for highly reversible lithium-ion batteries. J Mater Chem. 2012;22:20952–57.
[181] Chen KS, Balla I, Luu NS, Hersam MC. Emerging opportunities for two-dimensional materials in lithium-ion batteries. ACS Energy Lett. 2017;2:2026–34.
[182] Zhao Y, Peng L, Liu B, Yu G. Single-crystalline $LiFePO_4$ nanosheets for high-rate li-ion batteries. Nano Lett. 2014;14:2849–53.
[183] Zhao Q, Guo Z, Wu Y, Wang L, Han Z, Ma X, et al. Hierarchical flower-like spinel manganese-based oxide nanosheets for high-performance lithium ion battery. Sci China Mater. 2019;62:1385–92.
[184] Chen J, Zhao N, Zhao J, Li J, Guo FF, Li GD. Facile synthesis of $LiMn_2O_4$ microsheets with porous micro-nanostructure as high-rate cathode materials for Li-ion batteries. J Solid State Electrochem. 2018;22:331–8.
[185] Qiu S, Fang T, Zhu Y, Hua J, Chu H, Zou Y, et al. $Li_{1.2}Mn_{0.6}Ni_{0.2}O_2$ with 3D porous rod-like hierarchical micro/nanostructure for high-performance cathode material. J Alloy Compd. 2019;790:863–70.
[186] Li Y, Bai Y, Wu C, Qian J, Chen G, Liu L, et al. Three-dimensional fusiform hierarchical micro/nano $Li_{1.2}Ni_{0.2}Mn_{0.6}O_2$ with a preferred orientation (110) plane as a high energy cathode material for lithium-ion batteries. J Mater Chem A. 2016;4:5942–51.
[187] Deng YP, Yin ZW, Wu ZG, Zhang SJ, Fu F, Zhang T, et al. Layered/spinel heterostructured and hierarchical micro/nanostructured Li-rich cathode materials with enhanced electrochemical properties for Li-ion batteries. ACS Appl Mater Interfaces. 2017;9:21065–70.
[188] Li J, Luo S, Ding X, Wang Q, He P. Three-dimensional honeycomb-structural $LiAlO_2$-modified $LiMnPO_4$ composite with superior high rate capability as Li-ion battery cathodes. ACS Appl Mater Interfaces. 2018;10:10786–95.
[189] Qiu B, Yin C, Xia Y, Liu Z. Synthesis of three-dimensional nanoporous Li-rich layered cathode oxides for high

volumetric and power energy density lithium-ion batteries. ACS Appl Mater Interfaces. 2017;9:3661–6.
[190] Deng YP, Fu F, Wu ZG, Yin ZW, Zhang T, Li JT, et al. Layered/spinel heterostructured Li-rich materials synthesized by a one-step solvothermal strategy with enhanced electrochemical performance for Li-ion batteries. J Mater Chem A. 2015;4:257–63.
[191] Di Zhang Y, Li Y, Niu XQ, Wang DH, Zhou D, Wang CD, et al. A peanut-like hierarchical micro/nano-$Li_{1.2}Mn_{0.54}Ni_{0.18}Co_{0.08}O_2$ cathode material for lithium-ion batteries with enhanced electrochemical performance. J Mater Chem A. 2015;3:14291–97.
[192] Li W, Zhang H, Mu Y, Liu L, Wang Y. Unique synthesis of novel octahedral micro/nano-hierarchical $LiFePO_4$cages as an enhanced cathode material for lithium-ion batteries. J Mater Chem A. 2015;3:15661–7.
[193] Wu Y, Cao C, Zhu Y, Li J, Wang L. Cube-shaped hierarchical $LiNi_{1/3}Co_{1/3}Mn_{1/3}O_2$with enhanced growth of nanocrystal planes as high-performance cathode materials for lithium-ion batteries. J Mater Chem A. 2015;3:15523–8.
[194] Kim DH, Kim J. Synthesis of $LiFePO_4$ nanoparticles in polyol medium and their electrochemical properties. Electrochem Solid-State Lett. 2006;9:A439.
[195] Shin HC, Cho WI, Jang H. Electrochemical properties of carbon-coated $LiFePO_4$ cathode using graphite, carbon black, and acetylene black. Electrochim Acta. 2006;52:1472–6.
[196] Dominko R, Gaberscek M, Drofenik J, Bele M, Pejovnik S, Jamnik J. The role of carbon black distribution in cathodes for Li ion batteries. J Power Sources. 2003;119:770–3.
[197] Liu H, Cao Q, Fu LJ, Li C, Wu YP, Wu HQ. Doping effects of zinc on $LiFePO_4$ cathode material for lithium ion batteries. Electrochem commun. 2006;8:1553–7.
[198] Zhang WJ. Structure and performance of $LiFePO_4$ cathode materials: a review. J Power Sources. 2011;196:2962–70.
[199] Olivetti EA, Ceder G, Gaustad GG, Fu X, Chung D, Elgqvist E, et al. Lithium-ion battery supply chain considerations: analysis of potential bottlenecks in critical metals. Joule. 2016;1:229–43.
[200] Zhang L, Fu J, Zhang C. Mechanical composite of $LiNi_{0.8}Co_{0.15}Al_{0.05}O_2$/carbon nanotubes with enhanced electrochemical performance for lithium-ion batteries. Nanoscale Res Lett. 2017;12:376.
[201] Mollazadeh M, Habibi B. $LiFePO_4$/carbon/reduced graphene oxide nanostructured composite as a high capacity and fast rate cathode material for rechargeable lithium ion battery. Catal Lett. 2019;149:7–18.
[202] Wang Z, He W, Zhang X, Yue Y, Liu J, Zhang C, et al. Multilevel structures of $Li_3V_2(PO_4)_3$/phosphorus-doped carbon nanocomposites derived from hybrid V-MOFs for long-life and cheap lithium ion battery cathodes. J Power Sources. 2017;366:9–17.
[203] Qiao YQ, Feng WL, Li J, De Shen T. Ultralong cycling stability of carbon-nanotube/$LiFePO_4$ nanocomposites as electrode materials for lithium-ion batteries. Electrochim Acta. 2017;232:323–31.
[204] Meng X, IOP Conference Series: Earth and Environmental Science; 2019. Vol. 300, p. 42039.
[205] Chen Y, Tian Y, Qiu Y, Liu Z, He H, Li B, et al. Synthesis and superior cathode performance of sandwiched $LiMn_2O_4$@rGO nanocomposites for lithium-ion batteries. Mater Today Adv. 2019;1:100001.
[206] Dong J, Lin Y, Zong H, Yang H, Wang L, Dai Z. Three-dimensional architecture reduced graphene oxide–$LiFePO_4$ composite: preparation and excellent microwave absorption performance. Inorg Chem. 2019;58:2031–41.
[207] Dong B, Huang X, Yang X, Li G, Xia L, Chen G. Rapid preparation of high electrochemical performance $LiFePO_4$/C composite cathode material with an ultrasonic-intensified micro-impinging jetting reactor. Ultrason Sonochem. 2017;39:816–26.
[208] Khan S, Raj RP, Mohan TVR, Bhuvaneswari S, Varadaraju UV, Selvam P. Electrochemical performance of nano-$LiFePO_4$ embedded ordered mesoporous nitrogenous carbon composite as cathode material for Li-ion battery applications. J Electroanal Chem. 2019;848:113242.
[209] Liu J-YJ-H, Li X-X, Huang J-R, Li J-J, Zhou P, Liu J-YJ-H, et al. Three-dimensional graphene-based nanocomposites for high energy density Li-ion batteries. J Mater Chem A. 2017;5:5977–94.
[210] Ding YH, Ren HM, Huang YY, Chang FH, He X, Fen JQ, et al. Co-precipitation synthesis and electrochemical properties of graphene supported $LiMn_{1/3}Ni_{1/3}Co_{1/3}O_2$cathode materials for lithium-ion batteries. Nanotechnology. 2013;24:375401.
[211] Jiang R, Cui C, Ma H. Using graphene nanosheets as a conductive additive to enhance the rate performance of spinel $LiMn_2O_4$ cathode material. Phys Chem Chem Phys. 2013;15:6406–15.
[212] Xin Y, Qi L, Zhang Y, Zuo Z, Zhou H, Zhang X. Organic solvent-assisted free-standing $Li_2MnO_3LiNi_{1/3}Co_{1/3}Mn_{1/3}O_2$on 3D graphene as a high energy density cathode. Chem Commun. 2015;51:16381–4.
[213] Zhou Y, Lu J, Deng C, Zhu H, Chen GZ, Zhang S, et al. Nitrogen-doped graphene guided formation of monodisperse microspheres of $LiFePO_4$ nanoplates as the positive electrode material of lithium-ion batteries. J Mater Chem A. 2016;4:12065–72.
[214] Tao S, Huang WF, Wu GX, Zhu XB, Wang XB, Zhang M, et al. Performance enhancement of lithium-ion battery with $LiFePO_4$@C/RGO hybrid electrode. Electrochim Acta. 2014;144:406–11.
[215] Dhindsa KS, Mandal BP, Bazzi K, Lin MW, Nazri M, Nazri GA, et al. Enhanced electrochemical performance of graphene modified $LiFePO_4$ cathode material for lithium ion batteries. Solid State Ion. 2013;253:94–100.
[216] Venkateswara Rao C, Leela Mohana Reddy A, Ishikawa Y, Ajayan PM. $LiNi_{1/3}Co_{1/3}Mn_{1/3}O_2$–graphene composite as a promising cathode for lithium-ion batteries. ACS Appl Mater Interfaces. 2011;3:2966–72.
[217] Zhao N, Zhi X, Wang L, Liu Y, Liang G. Effect of microstructure on low temperature electrochemical properties of $LiFePO_4$/C cathode material. J Alloy Compd. 2015;645:301–8.
[218] Eftekhari A. $LiFePO_4$/C nanocomposites for lithium-ion batteries. J Power Sources. 2017;343:395–411.
[219] Oh J, Lee J, Hwang T, Kim JM, Dong Seoung K, Piao Y. Dual layer coating strategy utilizing N-doped carbon and reduced graphene oxide for high-performance $LiFePO_4$ cathode material. Electrochim Acta. 2017;231:85–93.
[220] Yi X, Zhang F, Zhang B, Yu WJ, Dai Q, Hu S, et al. (010) Facets dominated $LiFePO_4$ nano-flakes confined in 3D porous

graphene network as a high-performance Li-ion battery cathode. Ceram Int. 2018;44:18181–8.
[221] Zhao W, Xiong L, Xu Y, Li H, Ren Z. High performance Li_2MnO_3/rGO composite cathode for lithium ion batteries. J Power Sources. 2017;349:11–7.
[222] Yu X, Deng J, Yang X, Li J, Huang ZH, Li B, et al. A dual-carbon-anchoring strategy to fabricate flexible $LiMn_2O_4$ cathode for advanced lithium-ion batteries with high areal capacity. Nano Energy. 2020;67:104256.
[223] Wu F, Yan Y, Wang R, Cai H, Tong W, Tang H. Synthesis of $LiNi_{1/3}Mn_{1/3}Co_{1/3}O_2$@graphene for lithium-ion batteries *via* self-assembled polyelectrolyte layers. Ceram Int. 2017;43:7668–73.
[224] Guo L, Ren L, Wan L, Li J. Heterogeneous carbon/N-doped reduced graphene oxide wrapping $LiMn_{0.8}Fe_{0.2}PO_4$ composite for higher performance of lithium ion batteries. Appl Surf Sci. 2019;476:513–20.
[225] Kim YS, Lee SH, Son MY, Jung YM, Song HK, Lee H. Succinonitrile as a corrosion inhibitor of copper current collectors for overdischarge protection of lithium ion batteries. ACS Appl Mater Interfaces. 2014;6:2039–43.
[226] Xu H, Jin H, Qi Z, Guo Y, Wang J, Zhu Y, et al. Graphene foil as a current collector for NCM material-based cathodes. Nanotechnology. 2020;31:205710.
[227] Wu HCHC, Wu HCHC, Lee E, Wu NL. High-temperature carbon-coated aluminum current collector for enhanced power performance of $LiFePO_4$ electrode of Li-ion batteries. Electrochem commun. 2010;12:488–91.
[228] Wang R, Li W, Liu L, Qian Y, Liu F, Chen M, et al. Carbon black/graphene-modified aluminum foil cathode current collectors for lithium ion batteries with enhanced electrochemical performances. J Electroanal Chem. 2019;833:63–9.
[229] Loghavi MM, Askari M, Babaiee M, Ghasemi A. Improvement of the cyclability of Li-ion battery cathode using a chemical-modified current collector. J Electroanal Chem. 2019;841:107–10.
[230] Fritsch M, Standke G, Heubner C, Langklotz U, Michaelis A. 3D-cathode design with foam-like aluminum current collector for high energy density lithium-ion batteries. J Energy Storage. 2018;16:125–32.
[231] Wang M, Tang M, Chen S, Ci H, Wang K, Shi L, et al. Graphene-armored aluminum foil with enhanced anticorrosion performance as current collectors for lithium-ion battery. Adv Mater. 2017;29:1703882.
[232] Cao WJ, Greenleaf M, Li YX, Adams D, Hagen M, Doung T, et al. The effect of lithium loadings on anode to the voltage drop during charge and discharge of Li-ion capacitors. J Power Sources. 2015;280:600–5.
[233] Liu T, Feng Y, Duan Y, Cui S, Lin L, Hu J, et al. Formation of mono/bi-layer iron phosphate and nucleation of $LiFePO_4$ nano-crystals from amorphous 2D sheets in charge/discharge process for cathode in high-performance Li-ion batteries. Nano Energy. 2015;18:187–95.
[234] Nara H, Mukoyama D, Shimizu R, Momma T, Osaka T. Systematic analysis of interfacial resistance between the cathode layer and the current collector in lithium-ion batteries by electrochemical impedance spectroscopy. J Power Sources. 2019;409:139–47.
[235] Kretschmer K, Sun B, Xie X, Chen S, Wang G. A free-standing $LiFePO_4$–carbon paper hybrid cathode for flexible lithium-ion batteries. Green Chem. 2016;18:2691–8.
[236] Liu YH, Lin HH, Tai YJ. Binder-free carbon fiber-based lithium-nickel-manganese-oxide composite cathode with improved electrochemical stability against high voltage: effects of composition on electrode performance. J Alloy Compd. 2018;735:580–7.
[237] Wang CC, Lin YC, Chiu KF, Leu HJ, Ko TH. Advanced carbon cloth as current collector for enhanced electrochemical performance of lithium-rich layered oxide cathodes. ChemistrySelect. 2017;2:4419–27.
[238] Leijonmarck S, Cornell A, Lindbergh G, Wågberg L. Flexible nano-paper-based positive electrodes for Li-ion batteries – preparation process and properties. Nano Energy. 2013;2:794–800.
[239] Wang C, Li D, Too CO, Wallace GG. Electrochemical properties of graphene paper electrodes used in lithium batteries. Chem Mater. 2009;21:2604–6.
[240] Lu H, Behm M, Leijonmarck S, Lindbergh G, Cornell A. Flexible paper electrodes for li-ion batteries using low amount of TEMPO-oxidized cellulose nanofibrils as binder. ACS Appl Mater Interfaces. 2016;8:18097–106.
[241] Hu L, Choi JW, Yang Y, Jeong S, La Mantia F, Cui LF, et al. Highly conductive paper for energy-storage devices. Proc Natl Acad Sci U S A. 2009;106:21490–4.
[242] Kang YR, Li YL, Hou F, Wen YY, Su D. Fabrication of electric papers of graphene nanosheet shelled cellulose fibres by dispersion and infiltration as flexible electrodes for energy storage. Nanoscale. 2012;4:3248–53.
[243] Wang J, Li L, Wong CL, Madhavi S. Flexible single-walled carbon nanotube/polycellulose papers for lithium-ion batteries. Nanotechnology. 2012;23:495401.
[244] Pang Z, Sun X, Wu X, Nie Y, Liu Z, Yue L. Fabrication and application of carbon nanotubes/cellulose composite paper. Vacuum. 2015;122:135–42.
[245] Sharifi F, Ghobadian S, Cavalcanti FR, Hashemi N. Paper-based devices for energy applications. Renew Sustain Energy Rev. 2015;52:1453–72.
[246] Ventrapragada LK, Creager SE, Rao AM, Podila R. Carbon nanotubes coated paper as current collectors for secondary Li-ion batteries. Nanotechnol Rev. 2019;8:18–23.
[247] Li M, Lu J, Chen Z, Amine K. Macroscopic self-assembly: versatile hydrogel ensembles with macroscopic multidimensions (Adv. Mater. 52/2018). Adv Mater. 2018;30:1–24.
[248] Goodenough JB, Park KS. The Li-ion rechargeable battery: a perspective. J Am Chem Soc. 2013;135:1167–76.
[249] Xu K. Electrolytes and interphases in Li-ion batteries and beyond. Chem Rev. 2014;114:11503–618.
[250] Manthiram A. An outlook on lithium ion battery technology. ACS Cent Sci. 2017;3:1063–9.
[251] Zhou X, Wang F, Zhu Y, Liu Z. Graphene modified $LiFePO_4$ cathode materials for high power lithium ion batteries. J Mater Chem. 2011;21:3353–8.
[252] Purwanto A, Yudha CS, Ubaidillah U, Widiyandari H, Ogi T, Haerudin H. NCA cathode material: synthesis methods and performance enhancement efforts. Mater Res Express. 2018;5(12):122001.
[253] Fang R, Zhao S, Sun Z, Wang DW, Cheng HM, Li F. More reliable lithium-sulfur batteries: status, solutions and prospects. Adv Mater. 2017;29:1–25.

[254] Zheng Y, Zheng S, Xue H, Pang H. Metal–organic frameworks for lithium–sulfur batteries. J Mater Chem A. 2019;7:3469–91.
[255] Fu A, Wang C, Pei F, Cui J, Fang X, Zheng N. Recent advances in hollow porous carbon materials for lithium–sulfur batteries. Small. 2019;15:1804786.
[256] Yuan H, Liu T, Liu Y, Nai J, Wang Y, Zhang W, et al. A review of biomass materials for advanced lithium–sulfur batteries. Chem Sci. 2019;10:7484–95.
[257] Zhu J, Zhu P, Yan C, Dong X, Zhang X. Recent progress in polymer materials for advanced lithium-sulfur batteries. Prog Polym Sci. 2019;90:118–63.
[258] Liu M, Deng N, Ju J, Fan L, Wang L, Li Z, et al. A review: electrospun nanofiber materials for lithium-sulfur batteries. Adv Funct Mater. 2019;29:1905467.
[259] Rana M, Ahad SA, Li M, Luo B, Wang L, Gentle I, et al. Review on areal capacities and long-term cycling performances of lithium sulfur battery at high sulfur loading. Energy Storage Mater. 2019;18:289–310.
[260] He J, Manthiram A. A review on the status and challenges of electrocatalysts in lithium-sulfur batteries. Energy Storage Mater. 2019;20:55–70.
[261] Li T, Bai X, Gulzar U, Bai YJ, Capiglia C, Deng W, et al. A comprehensive understanding of lithium–sulfur battery technology. Adv Funct Mater. 2019;29:1901730.
[262] Guo J, Liu J. A binder-free electrode architecture design for lithium–sulfur batteries: a review. Nanoscale Adv. 2019;1:2104–22.
[263] Jana M, Xu R, Cheng XB, Yeon JS, Park JM, Huang JQ, et al. Rational design of two-dimensional nanomaterials for lithium–sulfur batteries. Energy Env Sci. 2020;13:1049–75.
[264] Mukkabla R, Buchmeiser MR. Cathode materials for lithium–sulfur batteries based on sulfur covalently bound to a polymeric backbone. J Mater Chem A. 2020;8:5379–94.
[265] Huang L, Li J, Liu B, Li Y, Shen S, Deng S, et al. Electrode design for lithium–sulfur batteries: problems and solutions. Adv Funct Mater. 2020;30:1910375.
[266] Zhang M, Chen W, Xue L, Jiao Y, Lei T, Chu J, et al. Adsorption-catalysis design in the lithium-sulfur battery. Adv Energy Mater. 2020;10:1903008.
[267] Fan L, Li M, Li X, Xiao W, Chen Z, Lu J. Interlayer material selection for lithium-sulfur batteries. Joule. 2019;3:361–86.
[268] Chen X, Hou T, Persson KA, Zhang Q. Combining theory and experiment in lithium–sulfur batteries: current progress and future perspectives. Mater Today. 2019;22:142–58.
[269] Ren W, Ma W, Zhang S, Tang B. Recent advances in shuttle effect inhibition for lithium sulfur batteries. Energy Storage Mater. 2019;23:707–32.
[270] Lim WG, Kim S, Jo C, Lee J. A comprehensive review of materials with catalytic effects in Li–S batteries: enhanced redox kinetics. Angew Chem - Int Ed. 2019;58:18746–57.
[271] Knoop JE, Ahn S. Recent advances in nanomaterials for high-performance Li–S batteries. J Energy Chem. 2020;47:86–106.
[272] Qi Q, Lv X, Lv W, Yang QH. Multifunctional binder designs for lithium-sulfur batteries. J Energy Chem. 2019;39:88–100.
[273] Li B, Xu H, Ma Y, Yang S. Harnessing the unique properties of 2D materials for advanced lithium–sulfur batteries. Nanoscale Horiz. 2019;4:77–98.
[274] Zhang L, Wang Y, Niu Z, Chen J. Advanced nanostructured carbon-based materials for rechargeable lithium-sulfur batteries. Carbon N Y. 2019;141:400–16.
[275] Zhong Y, Xia X, Deng S, Zhan J, Fang R, Xia Y, et al. Popcorn inspired porous macrocellular carbon: rapid puffing fabrication from rice and its applications in lithium-sulfur batteries. Adv Energy Mater. 2018;8:1701110.
[276] Jian Z, Li H, Cao R, Zhou H, Xu H, Zhao G, et al. Polydopamine-coated hierarchical tower-shaped carbon for high-performance lithium-sulfur batteries. Electrochim Acta. 2019;319:359–65.
[277] Li GC, Hu JJ, Li GR, Ye SH, Gao XP. Sulfur/activated-conductive carbon black composites as cathode materials for lithium/sulfur battery. J Power Sources. 2013;240:598–605.
[278] Zhong Y, Chao D, Deng S, Zhan J, Fang RY, Xia Y, et al. Confining sulfur in integrated composite scaffold with highly porous carbon fibers/vanadium nitride arrays for high-performance lithium-sulfur batteries. Adv Funct Mater. 2018;28:1706391.
[279] Ji X, Lee KT, Nazar LF. A highly ordered nanostructured carbon–sulphur cathode for lithium–sulphur batteries. Nat Mater. 2009;8:500–6.
[280] Perez Beltran S, Balbuena PB. Formation of multilayer graphene domains with strong sulfur–carbon interaction and enhanced sulfur reduction zones for lithium–sulfur battery cathodes. ChemSusChem. 2018;11:1970–80.
[281] Yang W, Yang W, Song A, Sun G, Shao G. 3D interconnected porous carbon nanosheets/carbon nanotubes as a polysulfide reservoir for high performance lithium–sulfur batteries. Nanoscale. 2018;10:816–24.
[282] Wang H, Yang Y, Liang Y, Robinson JT, Li Y, Jackson A, et al. Graphene-wrapped sulfur particles as a rechargeable lithium–sulfur battery cathode material with high capacity and cycling stability. Nano Lett. 2011;11:2644–7.
[283] Gueon D, Hwang JT, Yang SB, Cho E, Sohn K, Yang DK, et al. Spherical macroporous carbon nanotube particles with ultrahigh sulfur loading for lithium–sulfur battery cathodes. ACS Nano. 2018;12:226–33.
[284] Abdul Razzaq A, Yao Y, Shah R, Qi P, Miao L, Chen M, et al. High-performance lithium sulfur batteries enabled by a synergy between sulfur and carbon nanotubes. Energy Storage Mater. 2019;16:194–202.
[285] Moon S, Jung YH, Jung WK, Jung DS, Choi JW, Kim DK. Encapsulated monoclinic sulfur for stable cycling of Li-S rechargeable batteries. Adv Mater. 2013;25:6547–53.
[286] Zheng G, Lee SW, Liang Z, Lee HW, Yan K, Yao H, et al. Interconnected hollow carbon nanospheres for stable lithium metal anodes. Nat Nanotechnol. 2014;9:618–23.
[287] Ren J, Zhou Y, Wu H, Xie F, Xu C, Lin D. Sulfur-encapsulated in heteroatom-doped hierarchical porous carbon derived from goat hair for high performance lithium–sulfur batteries. J Energy Chem. 2019;30:121–31.
[288] Zhou S, Hu J, Liu S, Lin JX, Cheng J, Mei T, et al. Biomimetic micro cell cathode for high performance lithium–sulfur batteries. Nano Energy. 2020;72:104680.
[289] Fawaz W, Mosavati N, Abdelhamid E, Simon Ng KY. Synthesis of activated carbons derived from avocado shells as cathode materials for lithium–sulfur batteries. SN Appl Sci. 2019;1:289.

[290] Qin X, Wu J, Xu ZL, Chong WG, Huang JQ, Liang G, et al. Electrosprayed multiscale porous carbon microspheres as sulfur hosts for long-life lithium-sulfur batteries. Carbon N Y. 2019;141:16–24.
[291] Diéz N, Ferrero GA, Sevilla M, Fuertes AB. A simple and general approach for *in situ* synthesis of sulfur–porous carbon composites for lithium–sulfur batteries. Sustain Energy Fuels. 2019;3:3498–509.
[292] Wang Y, Zhang R, Chao Pang Y, Chen X, Lang J, Xu J, et al. Carbon@titanium nitride dual shell nanospheres as multifunctional hosts for lithium sulfur batteries. Energy Storage Mater. 2019;16:228–35.
[293] Hu L, Dai C, Liu H, Li Y, Shen B, Chen Y, et al. Double-shelled NiO-$NiCo_2O_4$ heterostructure@carbon hollow nanocages as an efficient sulfur host for advanced lithium-sulfur batteries. Adv Energy Mater. 2018;8:1800709.
[294] Li G, Lei W, Luo D, Deng YP, Wang D, Chen Z. 3D porous carbon sheets with multidirectional ion pathways for fast and durable lithium-sulfur batteries. Adv Energy Mater. 2018;8:1702381.
[295] Chen S, Huang X, Sun B, Zhang J, Liu H, Wang G. Multishelled hollow carbon nanospheres for lithium–sulfur batteries with superior performances. J Mater Chem A. 2014;2:16199–207.
[296] Sun Q, He B, Zhang XQ, Lu AH. Engineering of hollow core–shell interlinked carbon spheres for highly stable lithium–sulfur batteries. ACS Nano. 2015;9:8504–13.
[297] Yuan H, Zhang W, Guo Wang J, Zhou G, Zhuang Z, Luo J, et al. Facilitation of sulfur evolution reaction by pyridinic nitrogen doped carbon nanoflakes for highly-stable lithium-sulfur batteries. Energy Storage Mater. 2018;10:1–9.
[298] Kim J, Kang Y, Song SW, Suk J. Freestanding sulfur-graphene oxide/carbon composite paper as a stable cathode for high performance lithium-sulfur batteries. Electrochim Acta. 2019;299:27–33.
[299] Li W, Liang Z, Lu Z, Yao H, Seh ZW, Yan K, et al. A sulfur cathode with pomegranate-like cluster structure. Adv Energy Mater. 2015;5:1500211.
[300] Li Z, Zhang JT, Chen YM, Li J, Lou XW. Correlated compositional and mineralogical investigations at the Chang'e-3 landing site. Nat Commun. 2015;6:1–8.
[301] Chung SH, Chang CH, Manthiram A. A carbon-cotton cathode with ultrahigh-loading capability for statically and dynamically stable lithium–sulfur batteries. ACS Nano. 2016;10:10462–70.
[302] Lin C, Qu L, Li J, Cai Z, Liu H, He P, et al. Porous nitrogen-doped carbon/MnO coaxial nanotubes as an efficient sulfur host for lithium sulfur batteries. Nano Res. 2019;12:205–10.
[303] Kensy C, Härtel P, Maschita J, Dörfler S, Schumm B, Abendroth T, et al. Scalable production of nitrogen-doped carbons for multilayer lithium-sulfur battery cells. Carbon N Y. 2020;161:190–7.
[304] Zhou Y, Shu H, Zhou Y, Sun T, Han M, Chen Y, et al. Flower-like $Bi_4Ti_3O_{12}$/Carbon nanotubes as reservoir and promoter of polysulfide for lithium sulfur battery. J Power Sources. 2020;453:227896.
[305] Abualela S, Lv X, Hu Y, Abd-Alla MD. NiO nanosheets grown on carbon cloth as mesoporous cathode for High-performance lithium-sulfur battery. Mater Lett. 2020;268:127622.
[306] Radhika G, Subadevi R, Sivakumar M. Sulfur nested with mixture of MnO_2/AB composite as efficient host for high-performance Li–S batteries. J Chem Sci. 2020;132:53.
[307] Liu S, Li J, Yan X, Su Q, Lu Y, Qiu J, et al. Superhierarchical cobalt-embedded nitrogen-doped porous carbon nanosheets as two-in-one hosts for high-performance lithium-sulfur batteries. Adv Mater. 2018;30:1706895.
[308] Chen K, Sun Z, Fang R, Shi Y, Cheng HM, Li F. Metal-organic frameworks (MOFs)-derived nitrogen-doped porous carbon anchored on graphene with multifunctional effects for lithium-sulfur batteries. Adv Funct Mater. 2018;28:1707592.
[309] Zhang SS. Understanding of sulfurized polyacrylonitrile for superior performance lithium/sulfur battery. Energies. 2014;7:4588–600.
[310] Wang J, Yang J, Xie J, Xu N. A novel conductive polymer-sulfur composite cathode material for rechargeable lithium batteries. Adv Mater. 2002;14:963–5.
[311] He X, Shi Q, Zhou X, Wan C, Jiang C. *In situ* composite of nano SiO_2–P(VDF-HFP) porous polymer electrolytes for Li-ion batteries. Electrochim Acta. 2005;51:1069–75.
[312] He X, Ren J, Wang L, Pu W, Wan C, Jiang C. Electrochemical characteristics of sulfur composite cathode for reversible lithium storage. Ion (Kiel). 2009;15:477–81.
[313] Lai C, Gao XP, Zhang B, Yan TY, Zhou Z. Synthesis and electrochemical performance of sulfur/highly porous carbon composites. J Phys Chem C. 2009;113:4712–6.
[314] Guo J, Xu Y, Wang C. Sulfur-impregnated disordered carbon nanotubes cathode for lithium–sulfur batteries. Nano Lett. 2011;11:4288–94.
[315] Liu Y, Haridas AK, Cho KK, Lee Y, Ahn JH. Highly ordered mesoporous sulfurized polyacrylonitrile cathode material for high-rate lithium sulfur batteries. J Phys Chem C. 2017;121:26172–9.
[316] Wang W, Cao Z, Elia GA, Wu Y, Wahyudi W, Abou-Hamad E, et al. Recognizing the mechanism of sulfurized polyacrylonitrile cathode materials for Li–S batteries and beyond in Al–S batteries. ACS Energy Lett. 2018;3:2899–907.
[317] Wang X, Qian Y, Wang L, Yang H, Li H, Zhao Y, et al. Sulfurized polyacrylonitrile cathodes with high compatibility in both ether and carbonate electrolytes for ultrastable lithium–sulfur batteries. Adv Funct Mater. 2019;29:1902929.
[318] Xiang J, Guo Z, Yi Z, Zhang Y, Yuan L, Cheng Z, et al. Facile synthesis of sulfurized polyacrylonitrile composite as cathode for high-rate lithium-sulfur batteries. J Energy Chem. 2020;49:161–5.
[319] Bong Cho G, Seung Jeong J, Rang Chae M, Pil Noh J, Koo Cho K, Kwang Kim J, et al. Electrochemical properties of sulfurized poly-acrylonitrile (SPAN) cathode containing carbon fiber current collectors. Surf Coat Technol. 2017;326:443–9.
[320] Liu Y, Haridas AK, Lee Y, Cho KK, Ahn JH. Freestanding porous sulfurized polyacrylonitrile fiber as a cathode material for advanced lithium sulfur batteries. Appl Surf Sci. 2019;472:135–42.
[321] Choudhury S, Fischer D, Formanek P, Simon F, Stamm M, Ionov L. Porous carbon prepared from polyacrylonitrile for lithium-sulfur battery cathodes using phase inversion technique. Polym (Guildf). 2018;151:171–8.
[322] Kuo CJ, Weret MA, Hung HY, Tsai MC, Huang CJ, Su WN, et al. Sulfurized–poly(acrylonitrile) wrapped carbon sulfur

composite cathode material for high performance rechargeable lithium sulfur batteries. J Power Sources. 2019;412:670–6.
[323] Fan L, Chen S, Zhu J, Ma R, Li S, Podila R, et al. Simultaneous suppression of the dendrite formation and shuttle effect in a lithium–sulfur battery by bilateral solid electrolyte interface. Adv Sci. 2018;5:1700934.
[324] Liu Y, Yang D, Yan W, Huang Q, Zhu Y, Fu L, et al. Synergy of sulfur/polyacrylonitrile composite and gel polymer electrolyte promises heat-resistant lithium-sulfur batteries. iScience. 2019;19:316–25.
[325] Chen W-J, Li B-Q, Zhao C, Zhao M, Yuan T-Q, Sun R-C, et al. Electrolyte regulation towards stable lithium-metal anodes in lithium–sulfur batteries with sulfurized polyacrylonitrile cathodes. Angew Chem. 2020;132:10821–34.
[326] Peng HJ, Huang JQ, Cheng XB, Zhang Q. Lithium-sulfur batteries: review on high-loading and high-energy lithium-sulfur batteries (Adv. Energy Mater. 24/2017). Adv Energy Mater. 2017;7:1–54.
[327] Zhu K, Wang C, Chi Z, Ke F, Yang Y, Wang A, et al. How far away are lithium-sulfur batteries from commercialization. Front Energy Res. 2019;7:123.
[328] Bhargav A, He J, Gupta A, Manthiram A. Lithium-sulfur batteries: attaining the critical metrics. Joule. 2020;4:285–91.
[329] Zhao R, Liu J, Gu J. The effects of electrode thickness on the electrochemical and thermal characteristics of lithium ion battery. Appl Energy. 2015;139:220–9.
[330] Du Z, Wood DL, Daniel C, Kalnaus S, Li J. Understanding limiting factors in thick electrode performance as applied to high energy density Li-ion batteries. J Appl Electrochem. 2017;47:405–15.
[331] Li M, Carter R, Douglas A, Oakes L, Pint CL. Sulfur vapor-infiltrated 3D carbon nanotube foam for binder-free high areal capacity lithium–sulfur battery composite cathodes. ACS Nano. 2017;11:4877–84.
[332] Zhang H, Zhao W, Wu Y, Wang Y, Zou M, Cao A. Dense monolithic MOF and carbon nanotube hybrid with enhanced volumetric and areal capacities for lithium–sulfur battery. J Mater Chem A. 2019;7:9195–201.
[333] Rana M, Luo B, Kaiser MR, Gentle I, Knibbe R. The role of functional materials to produce high areal capacity lithium sulfur battery. J Energy Chem. 2020;42:195–209.
[334] Jia L, Wang J, Chen Z, Su Y, Zhao W, Wang D, et al. High areal capacity flexible sulfur cathode based on multi-functionalized super-aligned carbon nanotubes. Nano Res. 2019;12:1105–13.
[335] Liu Y, Yan Y, Li K, Yu Y, Wang Q, Liu M. A high-areal-capacity lithium–sulfur cathode achieved by a boron-doped carbon–sulfur aerogel with consecutive core–shell structures. Chem Commun. 2019;55:1084–7.
[336] Cho CS, Chang JY, Li CC. Highly symmetric gigaporous carbon microsphere as conductive host for sulfur to achieve high areal capacity for lithium–sulfur batteries. J Power Sources. 2020;451:227818.
[337] Abdul Razzaq A, Yuan X, Chen Y, Hu J, Mu Q, Ma Y, et al. Anchoring MOF-derived CoS_2 on sulfurized polyacrylonitrile nanofibers for high areal capacity lithium–sulfur batteries. J Mater Chem A. 2020;8:1298–306.
[338] Zhou G, Zhao Y, Manthiram A. Dual-confined flexible sulfur cathodes encapsulated in nitrogen-doped double-shelled hollow carbon spheres and wrapped with graphene for Li–S batteries. Adv Energy Mater. 2015;5(9):1402263.
[339] Pei F, Lin L, Ou D, Zheng Z, Mo S, Fang X, et al. *In situ* click chemistry generation of cyclooxygenase-2 inhibitors. Nat Commun. 2017;8:1–10.
[340] Carter R, Davis B, Oakes L, Maschmann MR, Pint CL. A high areal capacity lithium–sulfur battery cathode prepared by site-selective vapor infiltration of hierarchical carbon nanotube arrays. Nanoscale. 2017;9:15018–26.
[341] Liu F, Chiluwal S, Childress AS, Etteh C, Miller K, Washington M, et al. Conjugated polymers for photon-to-electron and photon-to-fuel conversions. ACS Appl Nano Mater. 2021;2021:60–92.
[342] Li X, Zhang Y, Wang S, Liu Y, Ding Y, He G, et al. Scalable high-areal-capacity Li–S batteries enabled by sandwich-structured hierarchically porous membranes with intrinsic polysulfide adsorption. Nano Lett. 2020;20:6922–9.
[343] Ghosh A, Kumar A, Roy A, Nguyen C, Ahuja A, Adil M, et al. Ultrathin lithium aluminate nanoflake-inlaid sulfur as a cathode material for lithium–sulfur batteries with high areal capacity. ACS Appl Energy Mater. 2020;3:5637–45.
[344] Bruce PG, Freunberger SA, Hardwick LJ, Tarascon JM. Li–O_2 and Li–S batteries with high energy storage. Nat Mater. 2012;11:19–29.
[345] Guo Y, Li H, Zhai T. Reviving lithium-metal anodes for next-generation high-energy batteries. Adv Mater. 2017;29:1700007.
[346] Whittingham MS. Electrical energy storage and intercalation chemistry. Science. 1976;192:1126–7.
[347] Tikekar MD, Choudhury S, Tu Z, Archer LA. Design principles for electrolytes and interfaces for stable lithium-metal batteries. Nat Energy. 2016;1:1–7.
[348] Liu J, Bao Z, Cui Y, Dufek EJ, Goodenough JB, Khalifah P, et al. Pathways for practical high-energy long-cycling lithium metal batteries. Nat Energy. 2019;4:180–6.
[349] Cheng XB, Zhang R, Zhao CZ, Zhang Q. Toward safe lithium metal anode in rechargeable batteries: a review. Chem Rev. 2017;117:10403–73.
[350] Xu W, Wang J, Ding F, Chen X, Nasybulin E, Zhang Y, et al. Lithium metal anodes for rechargeable batteries. Energy Env Sci. 2014;7:513–37.
[351] Kim J, Lee J, Yun J, Choi SH, Han SA, Moon J, et al. Functionality of dual-phase lithium storage in a porous carbon host for lithium-metal anode. Adv Funct Mater. 2020;30:1910538.
[352] Cheng XB, Hou TZ, Zhang R, Peng HJ, Zhao CZ, Huang JQ, et al. Dendrite-free lithium deposition induced by uniformly distributed lithium ions for efficient lithium metal batteries. Adv Mater. 2016;28:2888–95.
[353] Liu X, Liu J, Qian T, Chen H, Yan C. Novel organophosphate-derived dual-layered interface enabling air-stable and dendrite-free lithium metal anode. Adv Mater. 2020;32:1902724.
[354] Wang L, Fu S, Zhao T, Qian J, Chen N, Li L, et al. *In situ* formation of a LiF and Li–Al alloy anode protected layer on a Li metal anode with enhanced cycle life. J Mater Chem A. 2020;8:1247–53.
[355] McGrogan FP, Swamy T, Bishop SR, Eggleton E, Porz L, Chen X, et al. Compliant yet brittle mechanical behavior of Li_2S–P_2S_5 lithium-ion-conducting solid electrolyte. Adv Energy Mater. 2017;7:1602011.

[356] Zheng J, Engelhard MH, Mei D, Jiao S, Polzin BJ, Zhang JG, et al. Electrolyte additive enabled fast charging and stable cycling lithium metal batteries. Nat Energy. 2017;2(3):1–8.
[357] Li NW, Yin YX, Yang CP, Guo YG. An artificial solid electrolyte interphase layer for stable lithium metal anodes. Adv Mater. 2016;28:1853–8.
[358] Zhang XQ, Cheng XB, Zhang Q. Advances in interfaces between li metal anode and electrolyte. Adv Mater Interfaces. 2018;5:1701097.
[359] Wu S, Yi J, Zhu K, Bai S, Liu Y, Qiao Y, et al. A super-hydrophobic quasi-solid electrolyte for Li-O_2 battery with improved safety and cycle life in humid atmosphere. Adv Energy Mater. 2017;7:1601759.
[360] Huang Z, Ren J, Zhang W, Xie M, Li Y, Sun D, et al. Protecting the Li-metal anode in a Li-O_2 battery by using boric acid as an SEI-forming additive. Adv Mater. 2018;30:1803270.
[361] Lang J, Long Y, Qu J, Luo X, Wei H, Huang K, et al. One-pot solution coating of high quality LiF layer to stabilize Li metal anode. Energy Storage Mater. 2019;16:85–90.
[362] Luo W, Gong Y, Zhu Y, Li Y, Yao Y, Zhang Y, et al. Reducing interfacial resistance between garnet-structured solid-state electrolyte and Li-metal anode by a germanium layer. Adv Mater. 2017;29:1606042.
[363] Zhou B, Guo L, Zhang Y, Wang J, Ma L, Zhang WH, et al. A high-performance Li-O_2 battery with a strongly solvating hexamethylphosphoramide electrolyte and a LiPON-protected lithium anode. Adv Mater. 2017;29:1701568.
[364] Ryou MH, Lee DJ, Lee JN, Lee YM, Park JK, Choi JW. Excellent cycle life of lithium-metal anodes in lithium-ion batteries with mussel-inspired polydopamine-coated separators. Adv Energy Mater. 2012;2:645–50.
[365] Luo W, Zhou L, Fu K, Yang Z, Wan J, Manno M, et al. A thermally conductive separator for stable Li metal anodes. Nano Lett. 2015;15:6149–54.
[366] Zhang R, Chen X, Shen X, Zhang XQ, Chen XR, Cheng XB, et al. Coralloid carbon fiber-based composite lithium anode for robust lithium metal batteries. Joule. 2018;2:764–77.
[367] Luo Z, Liu C, Tian Y, Zhang Y, Jiang Y, Hu J, et al. Dendrite-free lithium metal anode with lithiophilic interphase from hierarchical frameworks by tuned nucleation. Energy Storage Mater. 2020;27:124–32.
[368] Yang T, Sun Y, Qian T, Liu J, Liu X, Rosei F, et al. Lithium dendrite inhibition *via* 3D porous lithium metal anode accompanied by inherent SEI layer. Energy Storage Mater. 2020;26:385–90.
[369] Li J, Zou P, Chiang SW, Yao W, Wang Y, Liu P, et al. A conductive-dielectric gradient framework for stable lithium metal anode. Energy Storage Mater. 2020;24:700–6.
[370] Yuan Y, Wu F, Bai Y, Li Y, Chen G, Wang Z, et al. Regulating Li deposition by constructing LiF-rich host for dendrite-free lithium metal anode. Energy Storage Mater. 2019;16:411–8.
[371] Zhang Y, Liu B, Hitz E, Luo W, Yao Y, Li Y, et al. A carbon-based 3D current collector with surface protection for Li metal anode. Nano Res. 2017;10:1356–65.
[372] Zhang Y, Luo W, Wang C, Li Y, Chen C, Song J, et al. High-capacity, low-tortuosity, and channel-guided lithium metal anode. Proc Natl Acad Sci U S A. 2017;114:3584–9.
[373] Shi P, Li T, Zhang R, Shen X, Cheng XB, Xu R, et al. Lithiophilic LiC_6 layers on carbon hosts enabling stable Li metal anode in working batteries. Adv Mater. 2019;31:1807131.
[374] Tsai CL, Roddatis V, Chandran CV, Ma Q, Uhlenbruck S, Bram M, et al. $Li_7La_3Zr_2O_{12}$ interface modification for Li dendrite prevention. ACS Appl Mater Interfaces. 2016;8:10617–26.
[375] Feng Y, Zhang C, Jiao X, Zhou Z, Song J. Highly stable lithium metal anode with near-zero volume change enabled by capped 3D lithophilic framework. Energy Storage Mater. 2020;25:172–9.
[376] Ye H, Xin S, Yin YX, Li JY, Guo YG, Wan LJ. Stable Li plating/stripping electrochemistry realized by a hybrid Li reservoir in spherical carbon granules with 3D conducting skeletons. J Am Chem Soc. 2017;139:5916–22.
[377] Liu L, Yin YX, Li JY, Wang SH, Guo YG, Wan LJ. Uniform lithium nucleation/growth induced by lightweight nitrogen-doped graphitic carbon foams for high-performance lithium metal anodes. Adv Mater. 2018;30:1706216.
[378] Jin C, Sheng O, Luo J, Yuan H, Fang C, Zhang W, et al. 3D lithium metal embedded within lithiophilic porous matrix for stable lithium metal batteries. Nano Energy. 2017;37:177–86.
[379] Sen Chi S, Liu Y, Song WL, Fan LZ, Zhang Q. Prestoring lithium into stable 3D nickel foam host as dendrite-free lithium metal anode. Adv Funct Mater. 2017;27:1700348.
[380] Jung JW, Cho SH, Nam JS, Kim ID. Current and future cathode materials for non-aqueous Li-air (O_2) battery technology – A focused review. Energy Storage Mater. 2020;24:512–28.
[381] Rahman MA, Wang X, Wen C. A review of high energy density lithium–air battery technology. J Appl Electrochem. 2014;44:5–22.
[382] Imanishi N, Yamamoto O. Perspectives and challenges of rechargeable lithium–air batteries. Mater Today Adv. 2019;4:100031.
[383] Lai J, Xing Y, Chen N, Li L, Wu F, Chen R. Electrolytes for rechargeable lithium–air batteries. Angew Chem - Int Ed. 2020;59:2974–97.
[384] Eftekhari A. Low voltage anode materials for lithium-ion batteries. Energy Storage Mater. 2017;7:157–80.
[385] Wagemaker M, Mulder FM. Properties and promises of nanosized insertion materials for Li-ion batteries. Acc Chem Res. 2013;46:1206–15.
[386] Moretti A, Kim GT, Bresser D, Renger K, Paillard E, Marassi R, et al. Investigation of different binding agents for nanocrystalline anatase TiO_2 anodes and its application in a novel, green lithium-ion battery. J Power Sources. 2013;221:419–26.
[387] Hong Z, Wei M. Layered titanate nanostructures and their derivatives as negative electrode materials for lithium-ion batteries. J Mater Chem A. 2013;1:4403–14.
[388] Chen Z, Belharouak I, Sun YK, Amine K. Titanium-based anode materials for safe lithium-ion batteries. Adv Funct Mater. 2013;23:959–69.
[389] Wang L, Tang C, Takeuchi KJ, Takeuchi ES, Marschilok AC. Synthesis and characterization of $Li_4Ti_5O_{12}$ anode materials with enhanced high-rate performance in lithium-ion batteries. MRS Adv. 2018;3:575–80. Materials Research Society
[390] Tojo T, Kawashiri S, Tsuda T, Kadowaki M, Inada R, Sakurai Y. Electrochemical performance of single $Li_4Ti_5O_{12}$ particle for lithium ion battery anode. J Electroanal Chem. 2019;836:24–9.
[391] Yi TF, Yang SY, Xie Y. Recent advances of $Li_4Ti_5O_{12}$as a promising next generation anode material for high power lithium-ion batteries. J Mater Chem A. 2015;3:5750–77.

[392] Li K, Zhang Y, Sun Y, Xu Y, Zhang H, Ye P, et al. Template-free synthesis of biomass-derived carbon coated $Li_4Ti_5O_{12}$ microspheres as high performance anodes for lithium-ion batteries. Appl Surf Sci. 2018;459:572–82.
[393] Zou S, Wang G, Zhang Y, Xue C, Chen H, Yang G, et al. Nanostructure and characterization of carbon composite with Al^{3+} and Mn^{4+} co-doped $Li_4Ti_5O_{12}$ as anodes for Li-ion batteries. J Alloy Compd. 2020;816:152609.
[394] Meng WW, Yan BL, Xu YJ. Scalable synthesis of Ti^{3+} self-doped $Li_4Ti_5O_{12}$ microparticles as an improved performance anode material for Li-ion batteries. J Alloy Compd. 2019;788:21–9.
[395] Sun L, Liu Z, Wang Z, Yang W, Yang J, Sun K, et al. The synergic effects of Ca and Sm co-doping on the crystal structure and electrochemical performances of $Li_{4-x}Ca_xTi_{5-x}Sm_xO_{12}$ anode material. Solid State Sci. 2019;87:110–7.
[396] Wang Z, Sun L, Yang W, Yang J, Sun K, Chen D, et al. Unveiling the synergic roles of Mg/Zr co-doping on rate capability and cycling stability of $Li_4Ti_5O_{12}$. J Electrochem Soc. 2019;166:A658–66.
[397] Meng WW, Xu YJ, Yan BL. *In situ* nano-sized spinel $Li_4Ti_5O_{12}$ powder fabricated by a one-step roasting process in molten salts. J Alloy Compd. 2018;732:784–91.
[398] Luo S, Zhang P, Yuan T, Ruan J, Peng C, Pang Y, et al. Molecular self-assembly of a nanorod N-$Li_4Ti_5O_{12}$/TiO_2/C anode for superior lithium ion storage. J Mater Chem A. 2018;6:15755–61.
[399] Odziomek M, Chaput F, Lerouge F, Rutkowska A, Świerczek K, Carlier D, et al. Impact of the synthesis parameters on the microstructure of nano-structured LTO prepared by glycothermal routes and 7Li NMR structural investigations. J Sol-Gel Sci Technol. 2019;89:225–33.
[400] Zhu X, Zhou S, Jiang X, Yao X, Xu X, Peng A, et al. High-performances of $Li_4Ti_5O_{12}$ anodes for lithium-ion batteries *via* modifying the Cu current collector through magnetron sputtering amorphous carbon. J Alloy Compd. 2020;830:154682.
[401] Pawlitzek F, Pampel J, Schmuck M, Althues H, Schumm B, Kaskel S. High-power lithium ion batteries based on preorganized necklace type $Li_4Ti_5O_{12}$/VACNT nano-composites. J Power Sources. 2016;325:1–6.
[402] Ji X, Liu H, Wu X, Lu Q, Li Z, Pang Y. Toward rational design of N-doped $Li_4Ti_5O_{12}$@carbon anode materials for high-performance lithium-ion batteries. Ion (Kiel). 2020;26:1211–20.
[403] Bon CY, Isheunesu P, Mwemezi M, Kim S, Afrifah VA, Hamenu L, et al. Mesoporous carbon/$Li_4Ti_5O_{12}$ nanoflakes composite anode material lithiated to 0.01 V. J Ind Eng Chem. 2019;80:551–7.
[404] Li D, Liu Y, Zhao W, Gao Y, Cao L, Liu Y, et al. Synthesis of Ce modified $Li_4Ti_5O_{12}$ using biomass as carbon source. J Electroanal Chem. 2019;851:113441.
[405] Li Y, Chen Q, Meng Q, Lei S, Li C, Li X, et al. One-step synthesis of a nanosized cubic Li_2TiO_3-coated Br, C, and N Co-doped $Li_4Ti_5O_{12}$ anode material for stable high-rate lithium-ion batteries. ACS Appl Mater Interfaces. 2019;11:25804–16.
[406] Meng T, Zeng R, Sun Z, Yi F, Shu D, Li K, et al. Chitosan-confined synthesis of N-doped and carbon-coated $Li_4Ti_5O_{12}$ nanoparticles with enhanced lithium storage for lithium-ion batteries. J Electrochem Soc. 2018;165:A1046–53.
[407] Liu Y, Zhao M, Xu H, Chen J. Fabrication of continuous conductive network for $Li_4Ti_5O_{12}$ anode by Cu-doping and graphene wrapping to boost lithium storage. J Alloy Compd. 2019;780:1–7.
[408] Yue J, Badaczewski FM, Voepel P, Leichtweiß T, Mollenhauer D, Zeier WG, et al. Critical role of the crystallite size in nanostructured $Li_4Ti_5O_{12}$ anodes for lithium-ion batteries. ACS Appl Mater Interfaces. 2018;10:22580–90.
[409] Zuo X, Zhu J, Müller-Buschbaum P, Cheng YJ. Silicon based lithium-ion battery anodes: a chronicle perspective review. Nano Energy. 2017;31:113–43.
[410] Li W, Sun X, Yu Y. Si-, Ge-, Sn-Based anode materials for lithium-ion batteries: from structure design to electrochemical performance. Small Methods. 2017;1:1600037.
[411] Ying H, Han WQ. Metallic Sn-based anode materials: application in high-performance lithium-ion and sodium-ion batteries. Adv Sci. 2017;4:1700298.
[412] Wu H, Cui Y. Designing nanostructured Si anodes for high energy lithium ion batteries. Nano Today. 2012;7:414–29.
[413] Szczech JR, Jin S. Nanostructured silicon for high capacity lithium battery anodes. Energy Env Sci. 2011;4:56–72.
[414] Ma D, Cao Z, Hu A. Si-Based anode materials for Li-ion batteries: a mini review. Nano-Micro Lett. 2014;6:347–58.
[415] Sun Y, Liu N, Cui Y. Promises and challenges of nanomaterials for lithium-based rechargeable batteries. Nat Energy. 2016;1:16071.
[416] Kalnaus S, Rhodes K, Daniel C. A study of lithium ion intercalation induced fracture of silicon particles used as anode material in Li-ion battery. J Power Sources. 2011;196:8116–24.
[417] Lee SW, McDowell MT, Berla LA, Nix WD, Cui Y. Fracture of crystalline silicon nanopillars during electrochemical lithium insertion. Proc Natl Acad Sci U S A. 2012;109:4080–5.
[418] McDowell MT, Ryu I, Lee SW, Wang C, Nix WD, Cui Y. Studying the kinetics of crystalline silicon nanoparticle lithiation with *in situ* transmission electron microscopy. Adv Mater. 2012;24:6034–41.
[419] Liu XH, Zhong L, Huang S, Mao SX, Zhu T, Huang JY. Size-dependent fracture of silicon nanoparticles during lithiation. ACS Nano. 2012;6:1522–31.
[420] Aghajamali M, Xie H, Javadi M, Kalisvaart WP, Buriak JM, Veinot JGC. Size and surface effects of silicon nanocrystals in graphene aerogel composite anodes for lithium ion batteries. Chem Mater. 2018;30:7782–92.
[421] Luo J, Zhao X, Wu J, Jang HD, Kung HH, Huang J. Crumpled graphene-encapsulated Si nanoparticles for lithium ion battery anodes. J Phys Chem Lett. 2012;3:1824–9.
[422] Lee JK, Smith KB, Hayner CM, Kung HH. Silicon nanoparticles–graphene paper composites for Li ion battery anodes. Chem Commun. 2010;46:2025–7.
[423] Zhou X, Yin Y-X, Wan L-J, Guo Y-G. Facile synthesis of silicon nanoparticles inserted into graphene sheets as improved anode materials for lithium-ion batteries. Chem Commun. 2012;48:2198–200.
[424] Zhou X, Yin Y-X, Wan L-J, Guo Y-G. Self-assembled nanocomposite of silicon nanoparticles encapsulated in graphene through electrostatic attraction for lithium-ion batteries. Adv Energy Mater. 2012;2:1086–90.
[425] Chang J, Huang X, Zhou G, Cui S, Hallac PB, Jiang J, et al. Multilayered Si nanoparticle/reduced graphene oxide hybrid

as a high-performance lithium-ion battery anode. Adv Mater. 2014;26:758–64.
[426] Wu H, Yu G, Pan L, Liu N, McDowell MT, Bao Z, et al. Stable Li-ion battery anodes by *in-situ* polymerization of conducting hydrogel to conformally coat silicon nanoparticles. Nat Commun. 2013;4:1943.
[427] Bai X, Yu Y, Kung HH, Wang B, Jiang J. Si@SiOx/graphene hydrogel composite anode for lithium-ion battery. J Power Sources. 2016;306:42–8.
[428] Hu L, Wu H, Gao Y, Cao A, Li H, McDough J, et al. Silicon-carbon nanotube coaxial sponge as Li-ion anodes with high areal capacity. Adv Energy Mater. 2011;1:523–7.
[429] Mu T, Zuo P, Lou S, Pan Q, Zhang H, Du C, et al. A three-dimensional silicon/nitrogen-doped graphitized carbon composite as high-performance anode material for lithium ion batteries. J Alloy Compd. 2019;777:190–7.
[430] Li L, Zuo Z, Shang H, Wang F, Li Y. *In-situ* constructing 3D graphdiyne as all-carbon binder for high-performance silicon anode. Nano Energy. 2018;53:135–43.
[431] Batmaz R, Hassan FM, Higgins D, Cano ZP, Xiao X, Chen Z. Highly durable 3D conductive matrixed silicon anode for lithium-ion batteries. J Power Sources. 2018;407:84–91.
[432] Wang F, Hu Z, Mao L, Mao J. Nano-silicon@soft carbon embedded in graphene scaffold: high-performance 3D free-standing anode for lithium-ion batteries. J Power Sources. 2020;450:227692.
[433] Eshetu GG, Figgemeier E. Confronting the challenges of next-generation silicon anode-based lithium-ion batteries: role of designer electrolyte additives and polymeric binders. ChemSusChem. 2019;12:2515–39.
[434] Zhao Y, Liu C, Sun Y, Yi R, Cai Y, Li Y, et al. 3D-structured multi-walled carbon nanotubes/copper nanowires composite as a porous current collector for the enhanced silicon-based anode. J Alloy Compd. 2019;803:505–13.
[435] Chakrapani V, Rusli F, Filler MA, Kohl PA. Silicon nanowire anode: improved battery life with capacity-limited cycling. J Power Sources. 2012;205:433–8.
[436] Franco Gonzalez A, Yang NH, Liu RS. Silicon anode design for lithium-ion batteries: progress and perspectives. J Phys Chem C. 2017;121:27775–87.
[437] Luo W, Chen X, Xia Y, Chen M, Wang L, Wang Q, et al. Surface and interface engineering of silicon-based anode materials for lithium-ion batteries. Adv Energy Mater. 2017;7:1701083.
[438] Liu L, Lyu J, Li T, Zhao T. Well-constructed silicon-based materials as high-performance lithium-ion battery anodes. Nanoscale. 2016;8:701–22.
[439] Agyeman DA, Song K, Lee GH, Park M, Kang YM. Carbon-coated Si nanoparticles anchored between reduced graphene oxides as an extremely reversible anode material for high energy-density Li-ion battery. Adv Energy Mater. 2016;6:1600904.
[440] Wu L, Yang J, Zhou X, Zhang M, Ren Y, Nie Y. Silicon nanoparticles embedded in a porous carbon matrix as a high-performance anode for lithium-ion batteries. J Mater Chem A. 2016;4:11381–7.
[441] Bie Y, Yu J, Yang J, Lu W, Nuli Y, Wang J. Porous microspherical silicon composite anode material for lithium ion battery. Electrochim Acta. 2015;178:65–73.
[442] Jung CH, Choi J, Kim WS, Hong SH. A nanopore-embedded graphitic carbon shell on silicon anode for high performance lithium ion batteries. J Mater Chem A. 2018;6:8013–20.
[443] Cho H, Kim K, Park CM, Jeong G. *In situ* fabrication of nano-hybrid carbon/polyamide film providing robust binding and conductive network in silicon anode for lithium-ion battery. J Power Sources. 2019;410–411:25–30.
[444] Zhang L, Guo H, Rajagopalan R, Hu X, Huang Y, Dou SX, et al. One-step synthesis of a silicon/hematite@carbon hybrid nanosheet/silicon sandwich-like composite as an anode material for Li-ion batteries. J Mater Chem A. 2016;4:4056–61.
[445] Zhang L, Rajagopalan R, Guo H, Hu X, Dou S, Liu H. A green and facile way to prepare granadilla-like silicon-based anode materials for Li-ion batteries. Adv Funct Mater. 2016;26:440–6.
[446] Zhang L, Wang C, Dou Y, Cheng N, Cui D, Du Y, et al. A yolk–shell structured silicon anode with superior conductivity and high tap density for full lithium-ion batteries. Angew Chem Int Ed. 2019;58:8824–8.
[447] Zhou Z, Pan L, Liu Y, Zhu X, Xie X. From sand to fast and stable silicon anode: synthesis of hollow Si@void@C yolk–shell microspheres by aluminothermic reduction for lithium storage. Chin Chem Lett. 2019;30:610–7.
[448] Zhu L, Chen Y, Wu C, Chu R, Zhang J, Jiang H, et al. Double-carbon protected silicon anode for high performance lithium-ion batteries. J Alloy Compd. 2020;812:151848.
[449] Liu N, Wu H, McDowell MT, Yao Y, Wang C, Cui Y. A yolk-shell design for stabilized and scalable Li-ion battery alloy anodes. Nano Lett. 2012;12:3315–21.
[450] Xing Y, Shen T, Guo T, Wang X, Xia X, Gu C, et al. A novel durable double-conductive core-shell structure applying to the synthesis of silicon anode for lithium ion batteries. J Power Sources. 2018;384:207–13.
[451] Feng X, Yang J, Bie Y, Wang J, Nuli Y, Lu W. Nano/micro-structured Si/CNT/C composite from nano-$SiO_2$for high power lithium ion batteries. Nanoscale. 2014;6:12532–9.
[452] Park BH, Jeong JH, Lee GW, Kim YH, Roh KC, Kim KB. Highly conductive carbon nanotube micro-spherical network for high-rate silicon anode. J Power Sources. 2018;394:94–101.
[453] Wang F, Chen G, Zhang N, Liu X, Ma R. Engineering of carbon and other protective coating layers for stabilizing silicon anode materials. Carbon Energy. 2019;1:219–45.
[454] Shelke MV, Gullapalli H, Kalaga K, Rodrigues MTF, Devarapalli RR, Vajtai R, et al. Facile synthesis of 3D anode assembly with Si nanoparticles sealed in highly pure few layer graphene deposited on porous current collector for long life Li-ion battery. Adv Mater Interfaces. 2017;4:1601043.
[455] Ababtain K, Babu G, Susarla S, Gullapalli H, Masurkar N, Ajayan PM, et al. Porous graphene current collectors filled with silicon as high-performance lithium battery anode. Mater Res Express. 2018;5:014004.
[456] Breitung B, Aguiló-Aguayo N, Bechtold T, Hahn H, Janek J, Brezesinski T. Embroidered copper microwire current collector for improved cycling performance of silicon anodes in lithium-ion batteries. Sci Rep. 2017;7:13010.
[457] Chiluwal S, Sapkota N, Rao AM, Podila R. Three-dimensional Si anodes with fast diffusion, high capacity, high rate capability, and long cycle life. ACS Appl Mater Interfaces. 2020;12:34763–70.

[458] Cen Y, Fan Y, Qin Q, Sisson RD, Apelian D, Liang J. Synthesis of Si anode with a microsized-branched structure from recovered Al scrap for use in Li-Ion batteries. J Power Sources. 2019;410–411:31–7.
[459] Prakash S, Zhang C, Park JD, Razmjooei F, Yu JS. Silicon core-mesoporous shell carbon spheres as high stability lithium-ion battery anode. J Colloid Interface Sci. 2019;534:47–54.
[460] Zhou Y, Yang Y, Hou G, Yi D, Zhou B, Chen S, et al. Stress-relieving defects enable ultra-stable silicon anode for Li-ion storage. Nano Energy. 2020;70:104568.
[461] Wang MS, Wang GL, Wang S, Zhang J, Wang J, Zhong W, et al. *In situ* catalytic growth 3D multi-layers graphene sheets coated nano-silicon anode for high performance lithium-ion batteries. Chem Eng J. 2019;356:895–903.
[462] Gao R, Tang J, Yu X, Tang S, Ozawa K, Sasaki T, et al. *In situ* synthesis of MOF-derived carbon shells for silicon anode with improved lithium-ion storage. Nano Energy. 2020;70:104444.
[463] Liu S, Zhang X, Yan P, Cheng R, Tang Y, Cui M, et al. Dual bond enhanced multidimensional constructed composite silicon anode for high-performance lithium ion batteries. ACS Nano. 2019;13:8854–64.
[464] Wang H, Fu J, Wang C, Wang J, Yang A, Li C, et al. A binder-free high silicon content flexible anode for Li-ion batteries. Energy Env Sci. 2020;13:848–58.
[465] Sitinamaluwa HS, Li H, Wasalathilake KC, Wolff A, Tesfamichael T, Zhang S, et al. Nanoporous SiO coated amorphous silicon anode material with robust mechanical behavior for high-performance rechargeable Li-ion batteries. Nano Mater Sci. 2019;1:70–6.
[466] Nealer R, Reichmuth D, Anair D. Cleaner cars from cradle to grave. J Union Concerned Sci. 2015;1–54.
[467] Emilsson E, Dahllöf L. Lithium-ion vehicle battery production. Stockholm, Sweden: IVL Swedish Environmental Research Institute; 2019.
[468] Hall D, Lutsey N. Effects of battery manufacturing on electric vehicle life-cycle greenhouse gas emissions. ICCT Brief. 2018;12.
[469] Masnadi MS, El-Houjeiri HM, Schunack D, Li Y, Englander JG, Badahdah A, et al. Global carbon intensity of crude oil production. Science. 2018;361:851–3.
[470] Fuel economy improvements are projected to reduce future gasoline use - Today in Energy - U.S. Energy Information Administration (EIA). https://www.eia.gov/todayinenergy/detail.php?id=31332#, (accessed 6 March 2021).
[471] Electricity generation, capacity, and sales in the United States - U.S. Energy Information Administration (EIA). https://www.eia.gov/energyexplained/electricity/electricity-in-the-us-generation-capacity-and-sales.php, (accessed 6 March 2021).
[472] Environment - U.S. Energy Information Administration (EIA) - U.S. Energy Information Administration (EIA). https://www.eia.gov/environment/emissions/co2_vol_mass.php, (accessed 6 March 2021).
[473] Peters JF, Baumann M, Zimmermann B, Braun J, Weil M. The environmental impact of Li-ion batteries and the role of key parameters – a review. Renew Sustain Energy Rev. 2017;67:491–506.
[474] Dunn JB, James C, Gaines L, Gallagher K, Dai Q, Kelly JC. Material and energy flows in the production of cathode and anode materials for lithium ion batteries. Argonne, IL (United States); 2015.
[475] Dunn JB, Gaines L, Kelly JC, James C, Gallagher KG. The significance of Li-ion batteries in electric vehicle life-cycle energy and emissions and recycling's role in its reduction. Energy Env Sci. 2015;8:158–68.
[476] Dunn JB, Gaines L, Kelly JC, Gallagher KG. REWAS 2016. Cham: Springer International Publishing; 2016. p. 73–79
[477] Wang Y, Yu Y, Huang K, Tang B. From the perspective of battery production: energy–environment–economy (3E) analysis of lithium-ion batteries in China. Sustainability. 2019;11:6941.
[478] Jacob J. The chalkboard: C rating of batteries: a misleading concept, C flux rather than C rate. Electrochem Soc Interface. 2018;27:42–3.
[479] Rowden B, Garcia-Araez N. A review of gas evolution in lithium ion batteries. Energy Rep. 2020;6:10–8.
[480] Leiva EPM. Modeling of lithium-ion batteries is becoming viral: where to go. J Solid State Electrochem. 2020;24:2117–20.
[481] Fan Y, Chen X, Legut D, Zhang Q. Modeling and theoretical design of next-generation lithium metal batteries. Energy Storage Mater. 2019;16:169–93.
[482] Zhao Y, Stein P, Bai Y, Al-Siraj M, Yang Y, Xu BX. A review on modeling of electro-chemo-mechanics in lithium-ion batteries. J Power Sources. 2019;413:259–83.
[483] Horstmann B, Single F, Latz A. Review on multi-scale models of solid-electrolyte interphase formation. Curr Opin Electrochem. 2019;13:61–9.
[484] Barré A, Deguilhem B, Grolleau S, Gérard M, Suard F, Riu D. A review on lithium-ion battery ageing mechanisms and estimations for automotive applications. J Power Sources. 2013;241:680–9.
[485] Zhu J, Wierzbicki T, Li W. A review of safety-focused mechanical modeling of commercial lithium-ion batteries. J Power Sources. 2018;378:153–68.
[486] Deng J, Bae C, Marcicki J, Masias A, Miller T. Safety modelling and testing of lithium-ion batteries in electrified vehicles. Nat Energy. 2018;3:261–6.
[487] Soto FA, Martinez de la Hoz JM, Seminario JM, Balbuena PB. Modeling solid-electrolyte interfacial phenomena in silicon anodes. Curr Opin Chem Eng. 2016;13:179–85.
[488] Joshi RP, Eickholt J, Li L, Fornari M, Barone V, Peralta JE. Machine learning the voltage of electrode materials in metal-ion batteries. ACS Appl Mater Interfaces. 2019;11:18494–503.
[489] Zhang Y, Tang Q, Zhang Y, Wang J, Stimming U, Lee AA. Identifying degradation patterns of lithium ion batteries from impedance spectroscopy using machine learning. Nat Commun. 2020;11:1706.
[490] Wang W, Brady NW, Liao C, Fahmy YA, Chemali E, West AC, et al. High-fidelity state-of-charge estimation of li-ion batteries using machine learning; 2019. arXiv preprint arXiv:1909.02448.
[491] Fan J, Fan J, Liu F, Qu J, Li R. A novel machine learning method based approach for Li-ion battery prognostic and health management. IEEE Access. 2019;7:160043–61.

[492] Jiang Z, Li J, Yang Y, Mu L, Wei C, Yu X, et al. Machine-learning-revealed statistics of the particle-carbon/binder detachment in lithium-ion battery cathodes. Nat Commun. 2020;11:2310.
[493] Liu Y, Zhao T, Ju W, Shi S. Materials discovery and design using machine learning. J Mater. 2017;3:159–77.
[494] Nonaka T, Kawaura H, Makimura Y, Nishimura YF, Dohmae K. *In situ* X-ray Raman scattering spectroscopy of a graphite electrode for lithium-ion batteries. J Power Sources. 2019;419:203–7.
[495] Liu T, Lin L, Bi X, Tian L, Yang K, Liu J, et al. *In situ* quantification of interphasial chemistry in Li-ion battery. Nat Nanotechnol. 2019;14:50–6.
[496] Krachkovskiy S, Trudeau ML, Zaghib K. Application of magnetic resonance techniques to the *in situ* characterization of li-ion batteries: a review. Mater (Basel). 2020;13:1694.
[497] Liu D, Shadike Z, Lin R, Qian K, Li H, Li K, et al. Review of recent development of *in situ*/operando characterization techniques for lithium battery research. Adv Mater. 2019;31:1806620.